Transcriptomic insights into the tritrophic plant–pathogen–mycoparasite interaction reveal coordinated reprogramming fungal secretomes and plant amino acid metabolism.

Kazuya Maeda[1], Mariko Kouda[1], Mai Ohara[1], Takumi Kawase[1], Koki Saito[1], Eishin Iwao[1], Hirotoshi Sushida[2], Tomoko Suzuki[3], Takuya Sumita[4], Yuichiro Iida[1]

[1] Laboratory of Plant Pathology, Faculty of Agriculture, Setsunan University, Nagaotoge-cho 45-1, Hirakata, Osaka 573-0101, Japan

[2] Institute of Food Research, National Agriculture and Food Research Organization (NARO), 2-1-12 Kannondai, Tsukuba, Ibaraki 305-8642, Japan

[3] Department of Chemical and Biological Sciences, Faculty of Science, Japan Women's University, Mejirodai 2-8-1, Bunkyo-ku, Tokyo 112-8681, Japan

[4] Department of biological resources management, School of Environmental Science, The University of Shiga Prefecture, Hasaka-cho 2500, Hikone, Shiga 522-8533

[*] **Correspondence to Y. Iida (yuichiro.iida@setsunan.ac.jp)**

ORCIDs: Kazuya Maeda: 0000-0001-9858-0362; Mariko Kouda: 0009-0000-8862-4202; Takumi Kawase: 0009-0006-2448-0805; Koki Saito: 0009-0007-5348-7739; Eishin Iwao: 0009-0000-6697-5378; Hirotoshi Sushida: 0000-0003-0631-6068; Tomoko Suzuki: 0000-0001-9561-968X; Takuya Sumita: 0000-0001-7980-018X; Yuichiro Iida: 0000-0001-5062-3255.

Short title: Transcriptomic analysis a plant–pathogen–mycoparasite system

Summary

- The tomato–*Cladosporium fulvum* (syn. *Fulvia fulva*) pathosystem has served as a model for the gene-for-gene concept of effectors and resistance proteins, but this binary framework does not include the potential influence of other microbial participants. Here we describe the dramatic changes in gene expression of all members of the tritrophic interaction among tomato, *C. fulvum*, and mycoparasitic fungus *Hansfordia pulvinata*.
- Transcriptomic analyses of the mycoparasite *H. pulvinata* during parasitism of *C. fulvum* on tomato *on planta* and *in vitro* revealed a dramatic upregulation of genes encoding small secreted proteins during mycoparasitism, notably, a Nep1-like protein (HpNlp1) lacked typical necrosis-inducing activity but induced the accumulation of antifungal compounds inhibiting spore germination of *C. fulvum.*
- Similarly, in *C. fulvum* parasitized by *H. pulvinata*, effector genes were highly expressed. Strikingly, effector protein Ecp2 was found to share structural similarity with pathogen killer toxin 4 proteins and had broad-spectrum antifungal activity, indicating a dual function in fungal competition and *Cf-ECP2*-mediated plant resistance.
- In tomato plants infected by *C. fulvum* parasitized by *H. pulvinata*, primary metabolism and defense-related genes were exclusively activated. These results suggest that in the tritrophic interaction, the mycoparasite simultaneously suppressed the pathogen and induced plant resistance. This study uncovers a multilayered molecular network in which the mycoparasite coordinates pathogen suppression and plant defense within the tritrophic interaction.

Keywords: mycoparasitism, Nep1-like protein, fungal effectors, Ecp2, antifungal proteins, amino acid metabolism, *Cladosporium fulvum*, *Hansfordia pulvinata*

INTRODUCTION

The biotrophic filamentous fungus *Cladosporium fulvum* Cooke [syn. *Fulvia fulva* (Cooke) Cif.] causes tomato leaf mold, a serious economic threat due to reducing fruit yield and quality and occasionally killing tomato plants (*Solanum lycopersicum* L.) (Thomma *et al*., 2005; de Wit *et al*., 2009). The fungus enters tomato leaves through open stomata in high humidity, colonizes the apoplast, and secretes numerous effector proteins to suppress plant immunity and facilitate infection (Mesarich *et al*., 2023). Commercial tomato cultivars have thus been bred with *Cf* resistance genes encoding receptor-like proteins (RLPs) with extracytoplasmic leucine-rich repeats from wild relatives (Mesarich *et al*., 2023). These RLPs recognize the corresponding *C. fulvum* effector proteins as virulence factors via a gene-for-gene relationship and trigger a hypersensitive response to restrict the growth of *C. fulvum* (Mesarich *et al*., 2023). However, *C. fulvum* rapidly evolves new races through mutation or loss of effector genes, thereby evading plant immunity (Iida *et al*., 2015; de la Rosa *et al*., 2024). The extensive use of resistant cultivars carrying only one or a few *Cf* genes has consequently led to the emergence of *C. fulvum* races that can overcome the resistance of the tomato plants (Luderer *et al*., 2002; Mesarich *et al*., 2014).

To date, over 100 effector genes have been identified in *C. fulvum* (Mesarich *et al*., 2018; Zaccaron & Stergiopoulos, 2024). Most encode small cysteine-rich proteins that contain an N-terminal signal peptide for secretion. The identified avirulence (Avr) and extracellular proteins (Ecp) effectors—such as Avr2, Avr4, Avr4E, Avr5, Avr9B, Avr9C, Ecp1, Ecp2, Ecp4, Ecp5, and Ecp6—exemplify the complex coevolution between fungal virulence factors and their cognate *Cf* immune receptors (Wulff *et al*., 2009; de la Rosa *et al*., 2024). Several effectors have been functionally characterized. Avr2 acts as a cysteine protease inhibitor that targets the apoplastic cysteine proteases Rcr3 and Pip1, thereby interfering with basal defense mechanisms conserved across solanaceous plants (Rooney *et al*., 2005; Shabab *et al*., 2008; Kourelis *et al*., 2020). Ecp6 suppresses chitin-triggered immunity by sequestering chitin oligomers released from the fungal cell wall, thus evading recognition by host pattern-recognition receptors (de Jonge *et al*., 2010). In contrast, Ecp2 induces cell death in both tomato and nonhost plants, suggesting a dual role as a potential virulence and avirulence factor (de Kock *et al*., 2004; de Wit *et al*., 2012). Notably, the Ecp2 effector contains an Hce2 (homolog of *Cladosporium fulvum Ecp2*) domain that is widely conserved across diverse fungal and bacterial taxa, implying a fundamental role for this domain in microbe–plant interactions (Stergiopoulos *et al*., 2012). However, the biochemical function of Ecp2 remains unclear. Of additional concern is that *C. fulvum* has developed resistance to fungicides (Yan

et al., 2008; Watanabe *et al*., 2017). The extensive breakdown of the resistance conferred by single *Cf* resistance genes and the emergence of fungicide-resistant strains emphasize the need for sustainable disease management strategies beyond conventional breeding and chemical approaches. To better understand the molecular basis of disease suppression, previous studies have primarily focused on the *C. fulvum*–tomato interaction within the framework of the gene-for-gene model, but tritrophic interactions involving additional microorganisms remain largely unexplored.

Hansfordia pulvinata (Berk. & M.A. Curtis) S. Hughes (syn. *Dicyma pulvinata*) is a mycoparasitic fungus serendipitously discovered on tomato leaves infected with *C. fulvum* in a greenhouse (Iida *et al*., 2018). It parasitizes *C. fulvum* and overgrows lesions, effectively suppressing disease progression, and has broad mycoparasitic activity against all known *C. fulvum* races (Iida *et al*., 2018). *H. pulvinata* recognizes *C. fulvum* hyphae, coils around them, and directly penetrates the hyphae, then forms intercellular structures within the host fungus (Peresse & Le Picard, 1980; Maeda *et al*., 2025). It also produces an eremophilane-type sesquiterpenoid, 13-deoxyphomenone (also known as sporogen-AO1), which has antifungal activity against *C. fulvum* (Tirilly *et al*., 1983; Maeda *et al*., 2025). The compound was initially identified as a sporulation-inducing factor in the koji mold *Aspergillus oryzae* (Tanaka *et al*., 1984a, 1984b). Comparative genomics recently revealed that the biosynthetic gene cluster for 13-deoxyphomenone (*DPH*) in *H. pulvinata* shares high synteny with that in *Aspergillus* species, suggesting horizontal gene transfer from an ancestral *Aspergillus* lineage (Maeda *et al*., 2025). Subsequently, *H. pulvinata* appears to have retained this gene cluster to support its mycoparasitic lifestyle, repurposing the endogeni

c sporogenesis function in *Aspergillus* species into exogenic antifungal activity that inhibits spore germination and hyphal elongation of *C. fulvum*. However, the molecular mechanisms underlying its mycoparasitism remain largely unknown. Since its mycoparasitism is not restricted to the phyllosphere (Maeda *et al*., 2025), comparative analyses of fungal–fungal interactions under different mycoparasitic conditions could provide new insights on the molecular basis of fungal host recognition and leaf-surface biocontrol mechanisms.

The *C. fulvum*–tomato interaction has long served as a valuable model for dissecting gene-for-gene dynamics in plant–pathogen systems (Mesarich et al. 2023.). Recent chromosome-scale genome assemblies of multiple *C. fulvum* races have substantially advanced our understanding of its genome structure and effector repertoire (Zaccaron *et al*., 2022; Zaccaron & Stergiopoulos, 2024). Nevertheless, the molecular basis governing fungal–fungal recognition and the tritrophic interactions with tomato plants remain largely uncharacterized. Here, we present transcriptomic evidence revealing how the mycoparasitic fungus *H. pulvinata* modulates both *C. fulvum* and tomato responses, providing molecular insights into the interplay among plant, pathogen and mycoparasite. These findings underscore the potential of the foliar mycoparasitic fungus as a promising biocontrol agent within complex plant–microbe ecosystems.

MATERIALS AND METHODS

Culture conditions for fungal strains and plants, treatments and assays

Fungal strains *H. pulvinata* 414-3 and *C. fulvum* CF301 were cultured on half-strength potato dextrose agar (PDA; BD Difco, Sparks, NJ, USA) or minimal medium (MM) agar (15 g sucrose, 5 g ammonium tartrate, 1 g NH_4NO_3, 1 g KH_2PO_4, 0.5 g $MgSO_4{\cdot}7H_2O$, 0.1 g NaCl, 0.1 g $CaCl_2{\cdot}H_2O$, 25 µL 0.2 mg mL^{-1} biotin, 15 g agar and 1 mL trace elements per liter) at 25 °C in the dark for 1 (*H. pulvinata*) and 2 weeks (*C. fulvum*) (Maeda *et al*., 2025). Spores were collected in distilled water and adjusted to 1×10^6 spores mL^{-1} using a hemocytometer. For *in vitro* assays, 100 µL of each spore suspension was spread onto nylon membranes on PDA and incubated for 1 (*H. pulvinata*) or 2 weeks (*C. fulvum*) (hereafter "*in vitro Hp*" and "*in vitro Cf*" conditions; Fig. **S1a**). For establishing the mycoparasitism *in vitro*, membranes bearing *C. fulvum* colonies were transferred to water agar (nutrient-poor) and sprayed with 1 mL of *H. pulvinata* spore suspension (1×10^6 spores mL^{-1}); plates were then incubated at 25 °C in the dark for 2 weeks (*in vitro Cf/Hp*; Fig. **S1a**).

140 Seedlings of tomato (*Solanum lycopersicum*) cv. Moneymaker (lacking all known *Cf*
141 resistance genes) were grown at 25 °C with 16 h light/8 h dark. Four-week-old plants were
142 either grown in high humidity as healthy controls for another 2 weeks (Healthy leaf; Fig.
143 **S1a**) or sprayed with approximately 3 mL of *C. fulvum* spore suspension (1×10^6 spores mL^{-}
144 ^{1}), then incubated in high humidity for 2 weeks until lesions developed ("*on planta Cf*"
145 interaction; Fig. **S1a**). For establishing the mycoparasitism on plants, plants with leaf mold
146 lesions were sprayed with approximately 3 mL of *H. pulvinata* spore suspension (1×10^6
147 conidia mL^{-1}) and incubated under high humidity at 25 °C for 2 weeks until lesions were
148 overgrown by white mycelia of *H. pulvinata* ("*on planta Cf/Hp*"; Fig. **S1a**).
149 *N. benthamiana* plants were grown for 4 weeks at 25 °C with a 16 h light/8 h dark.
150 *Arabidopsis thaliana* ecotype Col-0 seeds were surface-sterilized in 70% (v/v) ethanol for 1
151 min, rinsed three times with sterile distilled water, plated on Murashige and Skoog (MS) agar
152 (4.33 g MS basal medium (Sigma-Aldrich, St. Louis, MO, USA) and 20 g sucrose per liter,
153 pH 5.7), stratified at 4 °C in the dark for 1 month, then transferred to soil and grown for 5
154 weeks at 25 °C with 16 h light/8 h dark.
155
156 **Scanning electron microscopy (SEM)**
157 Details of the sample preparation and imaging procedures for SEM are described previously
158 (Maeda *et al*., 2025). Nylon membranes with fungal cultures were cut into about 5-mm
159 squares and fixed in 2.5% (v/v) glutaraldehyde in 100 mM cacodylate buffer (pH 7.4)
160 overnight at 4 °C, then 1% (w/v) osmium tetroxide in 100 mM cacodylate buffer (pH 7.4) for
161 1 h at room temperature. Samples were then dehydrated with a graded ethanol series, critical-
162 point dried in absolute ethanol using Leica EM CPD300 critical point dryer (Leica
163 Microsystems, Wetzlar, Germany), then mounted on stubs, coated with platinum-palladium,
164 and observed with a Hitachi SU-8220 scanning electron microscope (Tokyo, Japan).
165
166 **RNAseq and transcriptome analysis**
167 Three biological replicates were collected for each condition described above. Total RNA
168 was extracted using the RNeasy Plant Mini Kit (Qiagen, Hilden, Germany) according to the
169 manufacturer's instructions. Poly(A) mRNA was enriched with the NEBNext Poly(A)
170 mRNA Magnetic Isolation Module (New England Biolabs, Ipswich, MA, USA), and libraries
171 were prepared using the NEBNext Ultra II Directional RNA Library Prep Kit (NEB).
172 Libraries were sequenced on an Illumina NovaSeq 6000 platform (Illumina, San Diego, CA,
173 USA) with the PE150 kit (150 bp × 2 paired-end), producing 2 or 4 Gb of data per sample.

174 Raw read quality was assessed using FastQC Ver. 16.0.1
175 (bioinformatics.babraham.ac.uk/projects/fastqc). Low-quality bases and adapter sequences
176 were removed using Trimmomatic Ver. 0.39 (Bolger *et al*., 2014). Clean reads were aligned
177 to the respective reference genomes using HISAT2 Ver. 2.2.1; SAM files were converted to
178 BAM files with SamTools Ver. 1.18 (Li *et al*., 2009; Kim *et al*., 2019). Read counts were
179 generated using Rsubread Ver. 2.20.0. Differentially expressed genes (DEGs) were identified
180 with DESeq2 using thresholds of $|\log_2(\text{Fold-change})| \geq 1$ and adjusted *P*-value (padj) ≤ 0.05
181 (Love *et al*., 2014). Gene Ontology (GO) and KEGG (Kyoto Encyclopedia of Genes and
182 Genomes) enrichment analyses were performed using TBtools-II Ver. 2.119 (Aleksander *et*
183 *al*., 2023; Chen *et al*., 2023; Kanehisa *et al*., 2025). Data were visualized using SRplot (Tang
184 *et al*., 2023).
185
186 **Bioinformatic analysis**
187 Orthologous coding sequences were identified using OrthoFinder Ver. 2.5.5 (Emms & Kelly,
188 2019); 100 single-copy orthologs were selected for multiple sequence alignment. Sequence
189 alignments were generated using MAFFT Ver. 7.526 and subsequently trimmed with TrimAl
190 Ver. 1.4 (Katoh and Standley, 2013; Capella-Gutiérrez *et al*., 2009). Maximum-likelihood
191 phylogenetic trees were constructed with RAxML Ver. 8.2.12 using 1,000 bootstrap
192 replicates and the GTRCAT or PROTCATAUTO model (Stamatakis, 2014). The consistency
193 of tree topology was assessed using approximately unbiased (AU) tests (Shimodaira, 2002)
194 with 10,000 bootstrap replicates as previously described (Maeda *et al*., 2025). Signal peptides
195 were predicted with SignalP-6.0 (Teufel *et al*., 2022), candidate effectors with EffectorP-
196 fungi 3.0 (Sperschneider & Dodds, 2022), and subcellular localization with LOCALIZER
197 (Sperschneider *et al*., 2017). Secondary metabolite biosynthetic gene clusters were
198 identified using the fungal version of antiSMASH (Blin *et al*., 2023). GPI-anchored
199 proteins were predicted with NetGPI 1.1 (Gíslason *et al*., 2021), and carbohydrate-active
200 enzymes (CAZymes) were annotated using DIAMOND (Zhang *et al*., 2018). Default
201 parameters were used for all analyses unless otherwise specified.
202 For sequence similarity comparison, the EMBOSS Needle tool was used for pairwise
203 alignments (Madeira *et al*., 2024). Protein domains and motifs were predicted using the
204 Pfam database and the MEME Suite, respectively (Bailey *et al*., 2015; Mistry *et al*., 2021).
205 The 3D structures of proteins were predicted using ColabFold Ver. 1.5.5 (Mirdita *et al*.,
206 2022). Five models were generated with three iterative recycles each, and the models were
207 ranked according to their predicted local distance difference test (pLDDT) scores. The top-

208 ranked models were refined by AMBER energy minimization to resolve steric clashes and
209 improve stereochemical geometry. The resulting relaxed structures were used for subsequent
210 structural analyses. The structure of Ecp2 was analyzed using the Dali server to retrieve
211 structural homologs based on a non-redundant dataset clustered at 25% sequence identity
212 (PDB25), and structures were compared with TM-align (Zhang & Skolnick, 2005; Holm,
213 2022).
214
215 **Plasmid construction and protein expression**
216 Necrosis-inducing protein 1-Like (NLP) protein coding sequences were synthesized
217 (VectorBuilder, IL, USA), cloned into the pSfinx vector using a primer set (Table **S1**) and
218 NEBuilder HiFi assembly kit (NEB). The NLP genes were digested with EcoRI and
219 subcloned into the pPIC9K vector (Thermo Fisher Scientific, Waltham, MA, USA) for
220 expression in *Pichia pastoris* GS115 strain according to the manufacturer's instructions.
221 Transformants were selected on YPD medium (Fujifilm Wako, Osaka, Japan) containing
222 G418 (Fujifilm Wako) and confirmed by PCR using the primer set in Table **S1**. Expression
223 was induced by adding 5 mL of the pre-culture grown in BMGY (buffered minimal medium
224 supplemented with 1% glycerol, 2% peptone, and 1% yeast extract, 1.34% amino acid–free
225 yeast nitrogen base, 100 mM potassium phosphate buffer [pH 6.0], and 4×10^{-5}% D-biotin)
226 broth to 100 mL of BMMY (1.5 % [w/v] methanol instead of glycerol in BMGY), and
227 incubating the culture at 30 °C and 300 rpm for 96 h. Supernatants were collected by
228 centrifugation at 12,000 rpm for 10 min.
229 The gene *Ecp2* was PCR-amplified from genomic DNA of *C. fulvum* using a primer set
230 (Table **S1**) and cloned into pET-28b vector (Merck, Darmstadt, Germany) to express an N-
231 terminal His_6-tagged protein in *Escherichia coli* strain BL21(DE3). Expression was induced
232 in LB medium with 1 mM IPTG at 16 °C for 16 h. Cells were resuspended with 50 mM KPi
233 buffer (pH 7.4) and disrupted by sonication on ice (10 min: 2 s on–4 s off). Insoluble
234 fractions were solubilized in 10 mL of denaturing buffer (6 M guanidine hydrochloride, 10
235 mM Tris, 10 mM β-mercaptoethanol, pH 8.0) for 1 h at room temperature. Proteins were
236 purified in a Ni-affinity column HisTrap HP (Cytiva, Medemblik, The Netherlands),
237 concentrated using Vivaspin 6 (GE Healthcare, IL, USA) and quantified with a Qubit
238 fluorometer (Thermo Fisher Scientific). BL21(DE3) carrying empty pET-28b served as a
239 negative control.
240
241 **Western blot analysis**

242 All protein samples were heated at 95 °C for 10 min in sample buffer (1% SDS, 1% 2-
243 mercaptoethanol, 10 mM Tris–HCl, 20% (v/v) glycerol, pH 6.8) for denaturation. The
244 proteins were separated in 12% SDS-polyacrylamide gel and transferred onto PVDF
245 membrane (Bio-Rad, Hercules, CA, USA). Membranes were blocked with 5% skim milk in
246 TBS-T for 1 h before antibody incubation. Anti-His and anti-HA monoclonal antibodies (Cell
247 Signaling Technology, Danvers, MA, USA) were diluted in Can Get Signal solution 1
248 (1:10,000) (TOYOBO, Osaka, Japan) and used as primary antibodies to detect Ecp2 and
249 NLPs, respectively. Horseradish peroxidase-conjugated anti-rabbit antibody was diluted with
250 Can Get Signal solution 2 (1:2,000) (TOYOBO) for use as the secondary antibody. Signals
251 were visualized using an ECL western detection kit (GE Healthcare, Chicago, IL, USA) and
252 captured using a ChemiDoc imaging system (Bio-Rad).
253
254 **Functional assay of NLPs**
255 pSfinx plasmids were introduced into *Agrobacterium tumefaciens* strain GV3101 via
256 electroporation (Ma *et al*., 2012). Agrobacterium suspensions were adjusted to OD_{600} = 0.3 in
257 infiltration buffer (2.03 g $MgCl_2 \cdot 6H_2O$, 1.95 g MES, 500 μL of 200 mM acetosyringone per
258 liter, pH 5.6) and used to infiltrate leaves on 4-week-old plants of *N. benthamiana* by syringe
259 pressure. Leaves were monitored for necrosis 14 days after infiltration. Necrosis was
260 visualized by trypan blue staining (Ma *et al*., 2012) and quantified using ilastik (Ver. 1.4.1)
261 (Berg *et al*., 2019).
262 *P. pastoris* culture supernatant containing NLP proteins or BM medium (BMGY without
263 glycerol) was mixed at a 1:1 ratio with *C. fulvum* spore suspension (1×10^6 spores mL^{-1}). A
264 40 μL drop of each mixture was placed on a hydrophobic glass slide and incubated at room
265 temperature for 24 h. After incubation, germination of 200 spores per treatment was assessed
266 using a Nikon E600 light microscope (Tokyo, Japan). Culture supernatants containing NLP
267 proteins were collected from *P. pastoris* and used to syringe-infiltrate *N. benthamiana* leaves.
268 Twenty-four hours after infiltration, apoplastic fluid was collected by vacuum infiltration
269 with distilled water, followed by centrifugation (1,000 rpm, 10 min) (Joosten, 2012). Equal
270 volumes (10 μL) of *C. fulvum* spore suspension and apoplast fluid were then incubated at
271 room temperature for 24 h. A light microscope (Nikon) was then used to assess 200 spores
272 for germination.
273 Synthetic peptides of nlp24 (GenScript Biotech, Nanjing, China) were prepared in 500
274 nM stock solutions in dimethyl sulfoxide. Reactive oxygen species (ROS) were detected as

275 previously described with slight modifications (Yang *et al*., 2022). Leaf disks (0.125 cm^2) of
276 *N. benthamiana* were floated on sterile distilled water for 24 h, then treated with 10 μL of a
277 substrate mixture (5 μL of 10 mM L-012 [Fujifilm Wako] and 5 μL of protein or peptide).
278 Luminescence was recorded every 2 min for 40 min using a Tristar3 Multimode Reader
279 (Berthold Technologies, Bad Wildbad, Germany).
280
281 **Functional assays of Ecp2**
282 The abaxial side of *Cf-ECP2* tomato leaves was infiltrated with purified Ecp2 protein (final
283 concentration 1 μM) using a syringe. Leaves were incubated at 25 °C with 16 h light/8 h dark
284 for 6 d and checked for a hypersensitive response (HR). *In vitro* antifungal activity was
285 assayed as previously described (Chavarro-Carrero *et al*., 2024). Briefly, fungal spores were
286 suspended in 5% PDB containing 15 μM Ecp2 or empty vector control (1×10^4 spores mL^{-1}),
287 then 100 μL of the samples (three wells per sample) was incubated in wells of 96-well plates
288 at 25 °C for 4 days. For each well, five fields of view were photographed ($N = 15$). Fungal
289 growth was quantified and compared with the control using the Hybrid Cell Count module of
290 the BZ-800X (KEYENCE, Osaka, Japan).
291
292 **Statistical analyses**
293 R version 4.4.2 (R Core Team, 2024) was used for all analyses. The proportion of necrosis
294 relative to total leaf area in *N. benthamiana* was assessed using Dunnett's test, with the empty
295 vector as the control ($N = 3$). Spore germination rate of *C. fulvum* treated with NLPs was
296 analyzed by one-way ANOVA followed by Tukey's HSD test ($N = 3$). The spore germination
297 rate of *C. fulvum* in apoplastic fluid from *N. benthamiana* leaves treated with NLPs was
298 compared using the Mann–Whitney *U* test, with the buffer as the control ($N = 12$). The
299 relative growth rate of fungi and yeast treated with Ecp2 was compared using Student's *t*-test,
300 with the empty vector as the control ($N = 15$).
301
302 **RESULTS**
303 **Overview of RNA-seq datasets**
304 RNA was extracted from healthy control leaves, leaves infected with *C. fulvum* (*on planta*
305 *Cf*), and leaves with *C. fulvum* lesions overgrown by *H. pulvinata* (*on planta Cf/Hp*) (Fig. **1a**;
306 Fig. **S1a**). Because *H. pulvinata* parasitizes *C. fulvum* on leaf surfaces and on nutrient-poor
307 water agar (Iida *et al*., 2018; Maeda *et al*., 2025), fungal RNA was also extracted from *in*
308 *vitro* cultures of *H. pulvinata* alone (*in vitro Hp*), *C. fulvum* alone (*in vitro Cf*), and dual

309 cultures of *C. fulvum* and *H. pulvinata* (*in vitro Cf/Hp*) on water agar (Fig. **1a**; Fig. **S1a**).
310 Typical mycoparasitic growth characterized by white mycelium of *H. pulvinata* was observed
311 at 14 days after inoculation for the *on planta Cf/Hp* and *in vitro Cf/Hp* conditions (Fig. **1a**).
312 Microscopic observation confirmed that *H. pulvinata* penetrated *C. fulvum* hyphae (Fig. **1b**),
313 and that *C. fulvum* entered tomato leaves through stomata (Fig. **S1b**) as previously described
314 (Maeda *et al*., 2025). Also, hyphae of *H. pulvinata* elongated on the leaf surface and entered
315 stomata in the presence of *C. fulvum* (Fig. **S1b**). Raw reads were aligned to the reference
316 genome sequences of *H. pulvinata*, *C. fulvum* and tomato plants using HISAT2. The
317 proportion of uniquely mapped reads varied across samples, ranging from 10.3 % and 88.1 %
318 (Table **S2**), reflecting the multi organismal nature of several samples. Principal component
319 analysis (PCA) of normalized expression values revealed clear clustering of biological
320 replicates by treatment for each organism, indicating high within-treatment reproducibility
321 (Fig. **S1c**). In the transcriptome analysis, we identified DEGs using adjusted *p*-value (padj) ≤
322 0.05 and $|\log_2$ Fold-change$| \geq 1.0$. Functional enrichment of DEGs was performed using
323 KEGG pathway annotation to reveal biological processes that are positively and negatively
324 regulated during mycoparasitism.
325

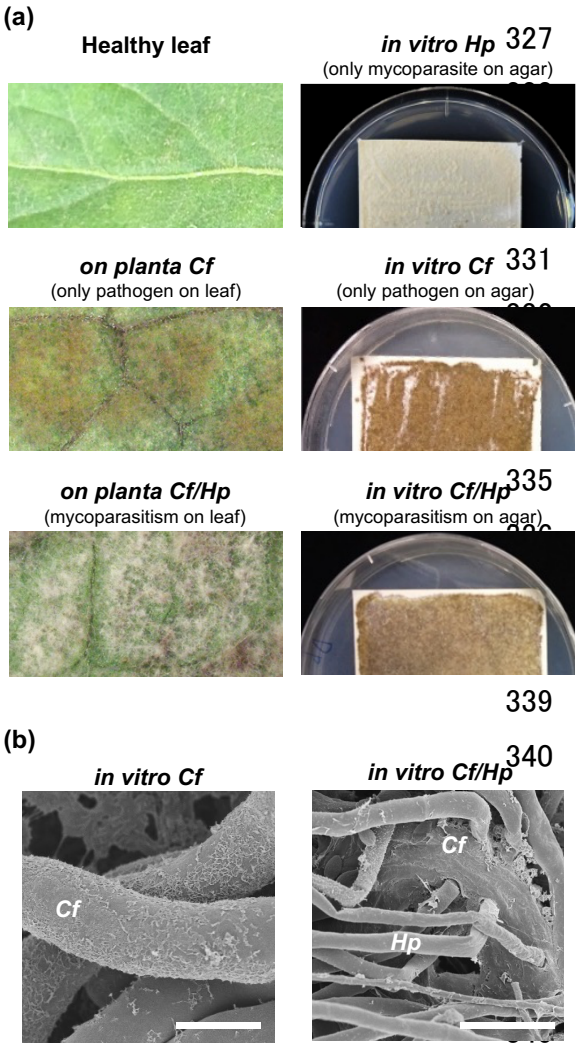

Fig. 1. *Cladosporium fulvum* parasitized by mycoparasitic fungus *Hansfordia pulvinata*. (a) Representative images of a healthy tomato leaf, lesions caused by *C. fulvum* (*on planta Cf*), and lesions covered by white mycelium of *H. pulvinata* (*on planta Cf/Hp*). Tomato plants were inoculated with *C. fulvum*, and lesions developed after 2 weeks. *H. pulvinata* was then inoculated onto the diseased leaves, and white mycelia appeared on the lesions a week later. *In vitro* cultures of *H. pulvinata* (*in vitro Hp*) and *C. fulvum* (*in vitro Cf*) on nylon membranes on water agar after transfer from PDA. *H. pulvinata* parasitized *C. fulvum* colonies on water agar (*in vitro Cf/Hp*). (b) Scanning electron micrographs of hyphae of *C. fulvum* grown *in vitro Cf* and *C. fulvum* parasitized by *H. pulvinata in vitro Cf/Hp*. *H. pulvinata* hyphae (*Hp*) have clearly penetrated *C. fulvum* hyphae (*Cf*). Bar indicates 10 µm.

Transcriptomic reprogramming in *H. pulvinata* during parasitisation of *C. fulvum*

Transcriptome analysis of *H. pulvinata* during parasitisation of *C. fulvum in vitro* (*in vitro Cf/Hp*) and *on planta* (*on planta Cf/Hp*) and the control (*in vitro Hp*) was used to identify DEGs involved in mycoparasitism based on gene annotation (Table **S3**). During parasitisation of *C. fulvum in vitro* (*in vitro Cf/Hp*), 1,336 genes were significantly upregulated and 738 genes were downregulated (Fig. **2a**), whereas 1,793 were upregulated and 2,086 were downregulated during parasitisation of *C. fulvum* grown on tomato leaves (*on planta Cf/Hp*). A core set of 891 upregulated DEGs was shared between the *in vitro Cf/Hp* and the *on planta Cf/Hp* conditions and a core set of 557 genes was downregulated and were mapped to 21 upregulated and 25 downregulated KEGG pathways (Fig. **2b**), suggesting in *H. pulvinata* a conserved transcriptional program was activated during parasitisation of *C. fulvum* both *in vitro* and *on planta*.

360 KEGG enrichment indicated reprogramming of primary and secondary metabolism in *H.*
361 *pulvinata* during parasitisation. KEGG pathways involved in secondary metabolism,
362 including steroids, terpenoids, and polyketides, were strongly upregulated. Genome mining
363 prediction revealed 33 putative secondary metabolite biosynthetic gene clusters in *H.*
364 *pulvinata*—12 non-ribosomal peptide synthetases (NRPSs), 10 type I polyketide synthases
365 (T1PKSs), 7 terpene synthetases, 3 fungal ribosomally synthesized and post-translationally
366 modified peptides (fungal-RiPPs), and an isocyanide—all of which underwent a marked
367 transcriptional change during parasitisation of *C. fulvum* (Table **S4**). Deoxyphomenone
368 biosynthesis (*DPH*) genes were also upregulated, consistent with *H. pulvinata* producing the
369 antifungal sesquiterpenoid 13-deoxyphomenone during parasitisation (Table **S4**) (Tirilly *et*
370 *al*., 1983; Maeda *et al*., 2025). Interestingly, multiple amino acid metabolism pathways were
371 consistently downregulated, despite *H. pulvinata* growing vegetatively during parasitisation
372 (Fig. **2b**). Given the central role of amino acids for protein synthesis and vegetative growth,
373 this KEGG pattern suggested that *H. pulvinata* may acquire amino acids derived from *C.*
374 *fulvum* or tomato plants to supplement its amino acid pool during mycoparasitism.

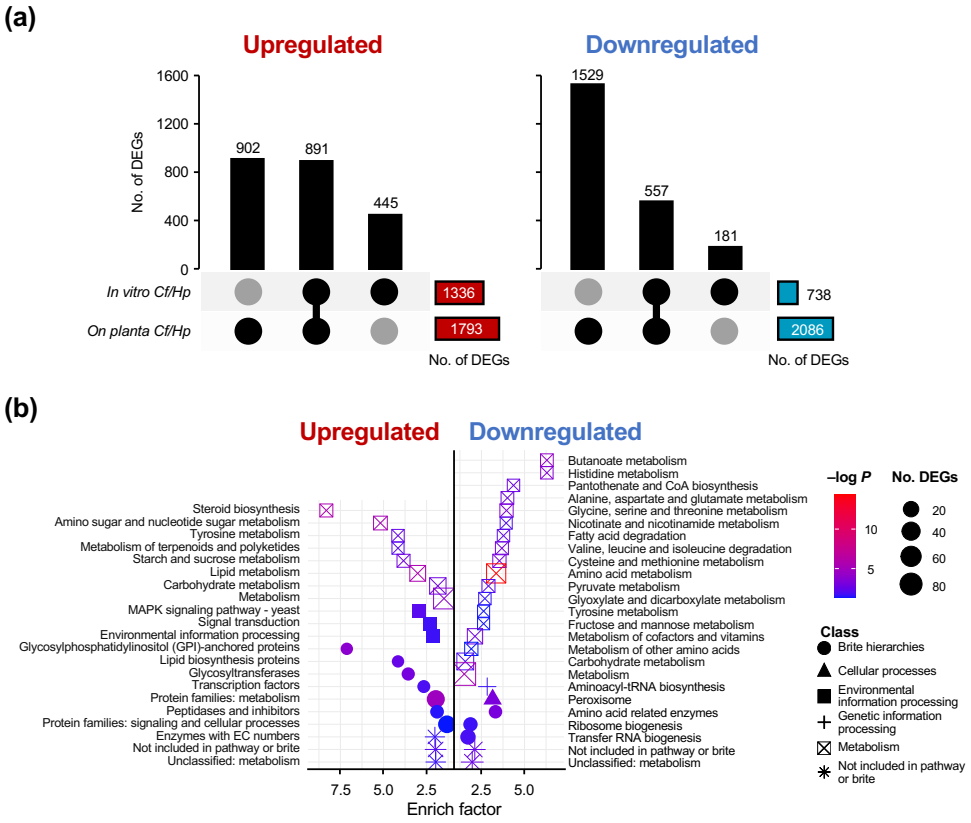

375

376 **Fig. 2. Differentially expressed genes (DEGs) and enriched KEGG pathways in**
377 **mycoparasite *Hansfordia pulvinata* during parasitisation of *C. fulvum in vitro* and *on***
378 ***planta*.** (a) UpSet plot of DEGs in the *in vitro* and *on planta* mycoparasitic conditions (*in*

379 *vitro Cf/Hp* and *on planta Cf/Hp*; Fig. 1a). Connected dots indicate shared DEGs; Black
380 single dots represent condition-specific DEGs. Vertical bars show the number of up- and
381 downregulated genes; colored horizontal bars indicate the total number of DEGs detected in
382 each interaction. (b) Bubble plot of KEGG pathway enrichment analysis based on the 891
383 and 557 shared DEGs shown in (a). Keys: color of symbols indicates significance level of
384 enrichment (–log adjusted *P*); size of symbol indicates the number of enriched DEGs in each
385 pathway; the symbol indicates the functional class of the enriched DEGs.
386
387 **Expression profile and functional analysis of small secreted proteins in *H. pulvinata***
388 A comparison of the genome structures of *H. pulvinata* with those of fungi and the
389 mycoparasite *Trichoderma atroviride* revealed that *H. pulvinata* had the smallest number of
390 genes encoding carbohydrate-active enzymes (CAZymes), and the highest number of genes
391 encoding secreted proteins (Fig. **S3**; Table **S3**). To analyze the secretome of *H. pulvinata*, we
392 filtered 891 DEGs commonly upregulated in both mycoparasitic interactions (*in vitro Cf/Hp*
393 and *on planta Cf/Hp*) and identified 165 genes encoding small secreted proteins (Fig. **3a**).
394 Although most of them could not be annotated for function, 27 were annotated as genes
395 previously reported to be associated with pathogenicity in plant pathogenic fungi, including
396 glycoside hydrolase, T2 family ribonuclease, EPL1-like protein (orthologous to Ecp45
397 effector protein in *C. fulvum*), hydrophobin, necrosis-inducing protein, KP4-type killer toxin
398 proteins, cutinase-like protein, superoxide dismutase protein, endoglucanase, and
399 metalloprotease (Table **S5**). We focused on a necrosis inducing protein (DIP_10004627),
400 designated *HpNLP1*, which is an Nep1-like protein (NLP) homologous to PsojNIP, because
401 *HpNLP1* showed a particularly high $-\log_{10}$ padj, indicating a high level of significance (Fig.
402 **3b**; Fig. **S4**). NLPs represent a widespread family of virulence-associated proteins in plant
403 pathogens that trigger necrosis and generation of ROS in host plants (Seidl & Van den
404 Ackerveken, 2019). Expression of *HpNLP1* increased 34-fold and 14-fold during
405 parasitisation of *C. fulvum in vitro* and *on planta*, respectively (Table **S5**). The NLP gene
406 *HpNLP2* (DIP_10008029) is also present in *H. pulvinata*, but its expression was unchanged
407 during parasitisation of *C. fulvum*.

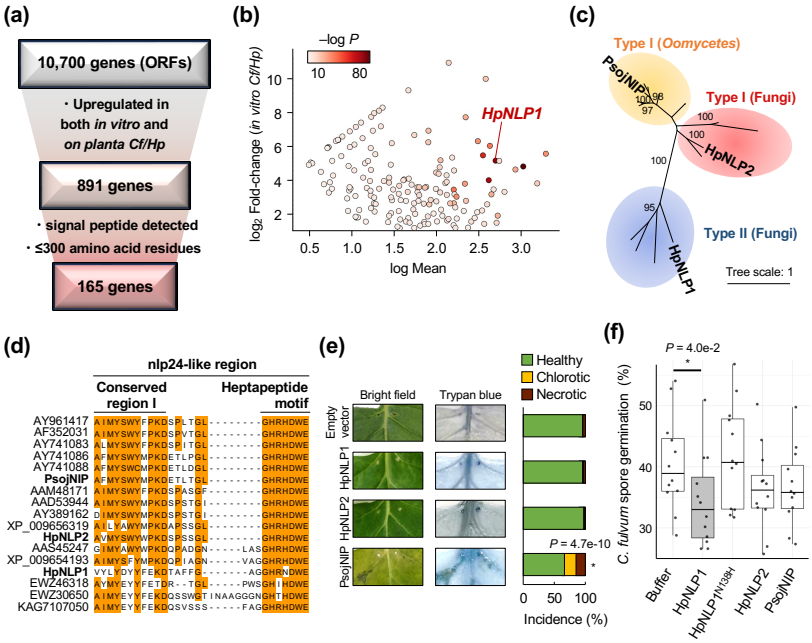

Fig. 3. A Nep1-like protein (NLP) secreted from the mycoparasite *Hansfordia pulvinata* induces a plant-mediated toxicity against spores of *Cladosporium fulvum*. (a) Workflow for identifying small secreted proteins synthesized in *H. pulvinata* during mycoparasitism. (b) MA plot for expression levels of 165 selected genes. Cutoff thresholds are $\log_2$ Fold-change (±1.0) for *in vitro Cf/Hp* interaction and log Mean (0.3). (c) Phylogenetic tree constructed based on NLP amino acid sequences using the maximum likelihood method with 1,000 bootstrap replicates. Type I and Type II have two and four cysteine residues, respectively. Proteins analyzed in this study are in bold. (d) Multiple sequence alignment of NLP using MAFFT. Conserved residues are highlighted in orange. (e) Transient expression assays of NLPs in *Nicotiana benthamiana* via agroinfiltration. Chlorosis and necrosis were assessed 14 days after infiltration by trypan blue staining. Similar results were obtained in three independent experiments; representative results are in Supplementary Fig. S5c. (f) Percentage germination of conidia of *C. fulvum* after 24-h treatment with apoplastic fluid from *N. benthamiana* leaves that had been infiltrated with different NLPs or buffer. Asterisks indicate significant differences between treatments determined using Dunnett's or the Mann–Whitney *U* test.

Phylogenetic analysis placed HpNlp1 and HpNlp2 within the type II and fungal type I clades, respectively, in NLPs (Fig. **3c**). HpNlp1 contained four cysteine residues predicted to form two disulfide bonds between positions 39–65 and 82–87 (Fig. **S4a** and **b**). Multiple sequence alignment showed that both HpNlp1 and HpNlp2 contained the conserved region I

430 and the C-terminal heptapeptide GHRHDWE motif; this conserved 24-amino-acid peptide
431 (nlp24) is recognized as a microbe- or pathogen-associated molecular pattern
432 (MAMP/PAMP) (Oome *et al*., 2014). The tryptophan (W) and proline (P) residues essential
433 for necrosis-inducing activity in the conserved region I (Zhou *et al*., 2012) were conserved in
434 HpNlp2 but replaced by tyrosine (Y) and glutamic acid (E) in HpNlp1 (Fig. **3d**), which was
435 the only NLP strongly expressed during mycoparasitism. In the heptapeptide motif of
436 HpNlp1, the second histidine (H) was replaced by asparagine (N) (Fig. **3d**). Structural
437 superposition of PsojNIP and HpNlp1 yielded a TM-score of 0.86 and a root mean square
438 deviation (RMSD) of 1.93 Å, demonstrating that despite mutations in the nlp24-like regions
439 of HpNlp1, the global protein structure was largely preserved, as indicated by these similar
440 values compared to the PsojNIP (Fig. **S4c**).
441 Recombinant proteins PsojNIP, HpNlp1 and HpNlp2 were produced in *P. pastoris* and
442 used to infiltrate *Nicotiana benthamiana* leaves. Western blot analysis of HpNlp1
443 demonstrated an additional band larger than the predicted molecular weight, suggesting dimer
444 formation (Fig. **S5a** and **b**). As previously reported, PsojNIP induced necrosis and chlorosis
445 (Qutob *et al*., 2002), whereas HpNlp1 and HpNlp2 did not trigger visible necrosis or ROS
446 accumulation (Fig. **3e**; Fig. **S5c** and **d**). The high expression of *HpNLP1* gene under *in vitro*
447 *Cf/Hp* condition, in the absence of the plant, suggested that HpNlp1 might directly suppress
448 *C. fulvum* growth. Contrary to this expectation, no such direct antifungal activity was
449 detected against *C. fulvum* spore germination and hyphal elongation (Fig. **S5e**). Remarkably,
450 however, apoplastic fluid—where *C. fulvum* develops—collected from *N.*
451 *benthamiana* leaves that had been infiltrated with HpNlp1 strongly suppressed *C. fulvum*
452 spore germination, whereas the protein with a point mutantation ($HpNlp1^{N138H}$) failed to elicit
453 antifungal activity (Fig. **3f**). Neither of the nlp24 peptides of HpNlp1 and $HpNlp1^{N138H}$
454 induced RLP23-mediated resistance (Fig. **S5f**). These findings together demonstrated that
455 HpNlp1 diverges from typical necrosis-inducing NLPs in plant pathogens, inducing the
456 accumulation of apoplastic antifungal substances that suppress *C. fulvum* spore germination
457 instead of promoting host cell death.
458
459 **Transcriptomic responses of pathogen *C. fulvum* parasitized by *H. pulvinata***
460 Next, we investigated the DEGs of *C. fulvum* through KEGG pathway analysis after tomato
461 was infected by *C. fulvum* (*on planta Cf*), dual infection on tomato leaves (*on planta Cf/Hp*),
462 and dual culture on agar medium (*in vitro Cf/Hp*) (Fig. **1a**). DEGs in *C. fulvum* were
463 identified during parasitisation relative to the *in vitro Cf* control, in which the fungus was

464 cultured on water agar. A total of 1,902 genes were upregulated and 1,783 genes were
465 downregulated when *C. fulvum* infected tomato leaves (*on planta Cf*) (Fig. **4a**). Under the
466 two mycoparasitic conditions, 2,195 upregulated and 2,435 downregulated genes were
467 detected *on planta Cf/Hp*, and 1,479 upregulated and 845 downregulated were detected *in*
468 *vitro Cf/Hp*. We identified 363 upregulated and 158 downregulated genes shared between the
469 two mycoparasitic conditions (*in vitro Cf/Hp* and *on planta Cf/Hp*), indicating a conserved
470 transcriptional response to *H. pulvinata* attack. KEGG enrichment analysis assigned these
471 shared DEGs to seven upregulated and three downregulated pathways, revealing strong
472 activation of protein folding and processing pathways in *C. fulvum* during parasitisation by *H.*
473 *pulvinata* (Fig. **4b**). Conversely, genes involved in amino acid metabolism were consistently
474 downregulated, as was also observed in *H. pulvinata*, suggesting coordinated suppression of
475 primary metabolism in this fungus-fungus interaction.

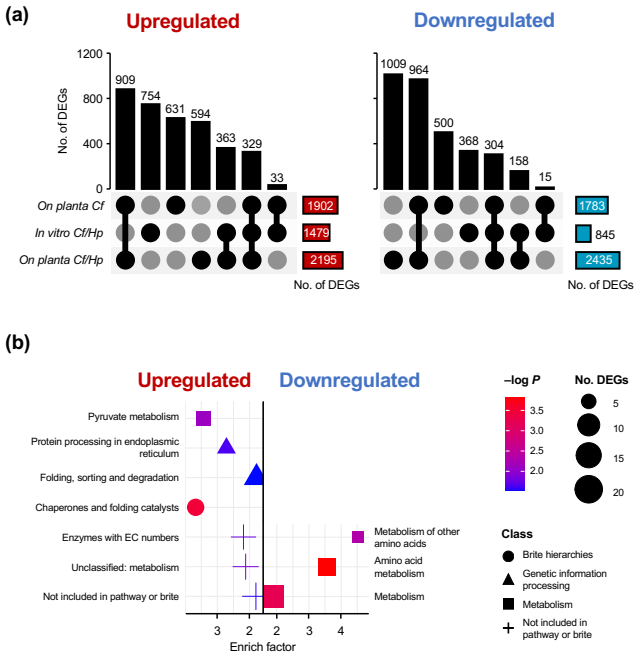

476

477 **Fig. 4. Differentially expressed genes (DEGs) and enriched KEGG pathways in the**
478 **pathogen *Cladosporium fulvum*.** (a) UpSet plot showing DEGs identified in the *on planta*
479 *Cf, in vitro Cf/Hp,* and *on planta Cf/HP* conditions (see Fig. 1A). Connected dots indicate
480 shared DEGs; Black single dots represent condition-specific DEGs. Vertical bars show the
481 numbers of up- and downregulated genes; colored horizontal bars indicate the total number of
482 DEGs detected in each condition. (b) Bubble plot of KEGG pathway enrichment analysis
483 based on the 363 and 158 shared DEGs shown in (a). Keys: color of symbols indicates
484 significant level of enrichment (–log adjusted *P*); size of symbol indicates the number of

485 enriched DEGs in each pathway; the different symbols represent functional classes of the
486 enriched DEGs.
487
488 In *C. fulvum*, protein folding and processing pathways were strongly activated when
489 parasitized by *H. pulvinata* (Fig. **4a**). These responses are indicative of endoplasmic
490 reticulum (ER) stress and accumulation of misfolded proteins, phenomena often triggered by
491 exposure to antifungal compounds (Chaillot *et al*., 2015). Similar to the results in the
492 mycoparasite *H. pulvinata*, the downregulation of secondary metabolism-related genes
493 suggested that *C. fulvum* reallocated resources from the production of secondary metabolites
494 to survive and mitigate stress. The expression profiles of DEGs detected in *C. fulvum* were
495 further analyzed based on functional classification as previously reported by Zaccaron &
496 Stergiopoulos (2024). Among the 42 genes associated with secondary metabolite
497 biosynthesis, 15 (35.7 %) and 18 (42.8 %) were downregulated in the *on planta Cf* and *on*
498 *planta Cf/Hp* interaction, respectively (Fig. **5a**; Table **S6**). Thirteen genes, including *PKS6*
499 (CLAFUR5_12905), a key enzyme in cladofulvin biosynthesis (Griffiths *et al*., 2018), were
500 consistently downregulated in both interactions.
501 In contrast, the category of small secreted proteins had the highest number of upregulated
502 DEGs, including numerous known or predicted effectors (Fig. **5a**). An expression heatmap of
503 effector genes showed that, as expected, the majority of the 106 effector genes were highly
504 expressed during infection of tomato by *C. fulvum* (*on planta Cf*) (Fig. **5b**). Expression of
505 effector genes are generally low on rich synthetic media (Mesarich *et al*., 2014); however
506 surprisingly, 56 effector genes were upregulated in the *in vitro* coculture of *C. fulvum* and *H.*
507 *pulvinata* (*in vitro Cf/Hp*) (Fig. **5b**). On tomato leaves, effector expression in *C. fulvum*
508 remained high regardless of the presence of *H. pulvinata* (Fig. **S6**). These results suggested
509 that *C. fulvum* effectors may play a defensive role, acting as countermeasures against
510 mycoparasitic attack by *H. pulvinata* or are upregulated due to nitrogen limitation caused by
511 parasitisation by *H. pulvinata.* To investigate this possibility, we conducted an AMAPEC
512 analysis, which predicts antimicrobial proteins based on 3D-structural signatures (Mesny *et*
513 *al*., 2024). Of the 56 effector genes that were upregulated under the *in vitro Cf/Hp* condition,
514 34 were predicted to possess antimicrobial activity, suggesting that many effectors may act as
515 antifungal proteins (Fig. **5c**; Table **S7**). Among these, we focused on the effector Ecp2, which
516 is known to trigger a hypersensitive response (HR) in tomato cultivars carrying the *Cf-ECP2*
517 resistance gene.

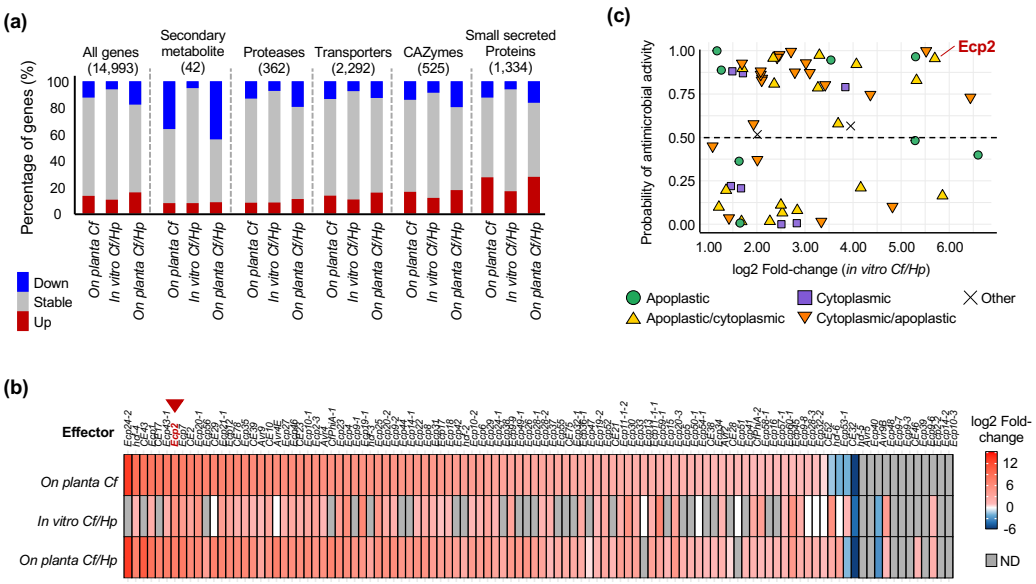

Fig. 5. Effector genes in the pathogen *Cladosporium fulvum* were highly expressed during parasitisation by *Hansfordia pulvinata.* (a) Functional classification of DEGs identified for the *on planta Cf*, *in vitro Cf/Hp* and *on planta Cf/Hp* interactions. Red: upregulated, stable: grey, blue: downregulated. The number of genes assigned to each category is in parentheses. (b) Heatmap showing expression profiles of effector genes. The red-to-blue gradient represents up- and downregulated expression, respectively. Genes with an adjusted *P*-value ≥0.05 are indicated in gray as not detected (ND). Red arrowhead indicates *Ecp2*. (c) Antimicrobial activity prediction for 56 effector genes upregulated during the *in vitro Cf/Hp* interaction (determined using the AMAPEC program). Symbols denote protein location predicted by EffectorP-fungi 3.0.

Structural and functional similarity between *C. fulvum* Ecp2 effector and antifungal killer toxin 4 proteins

The Alphafold2-predicted structure of Ecp2 yielded high confidence scores, with a pLDDT of 91.3 and a pTM of 0.872, indicating reliable local and global structures (Fig. **6a**). Structural similarity search using the DALI server identified two killer toxin 4 (KP4)-like proteins, ZtKP4 in *Zymoseptoria tritici* and UmVKP4 in *Ustilago maydis*, despite their low amino acid sequence similarity (2.9 to 36.9%) (Table **S8**). Comparative structural analysis showed that the overall arrangement of the α-helices and multiple β-sheets were conserved among these proteins (Fig. **6a** and **S7a**). The TM-scores for Ecp2 relative to ZtKP4 and UmVKP4 were 0.81 and 0.59, respectively, supporting that Ecp2 had the same structural fold as the KP4 protein family according to the SCOP and CATH classification criteria (Fig. **6b**).

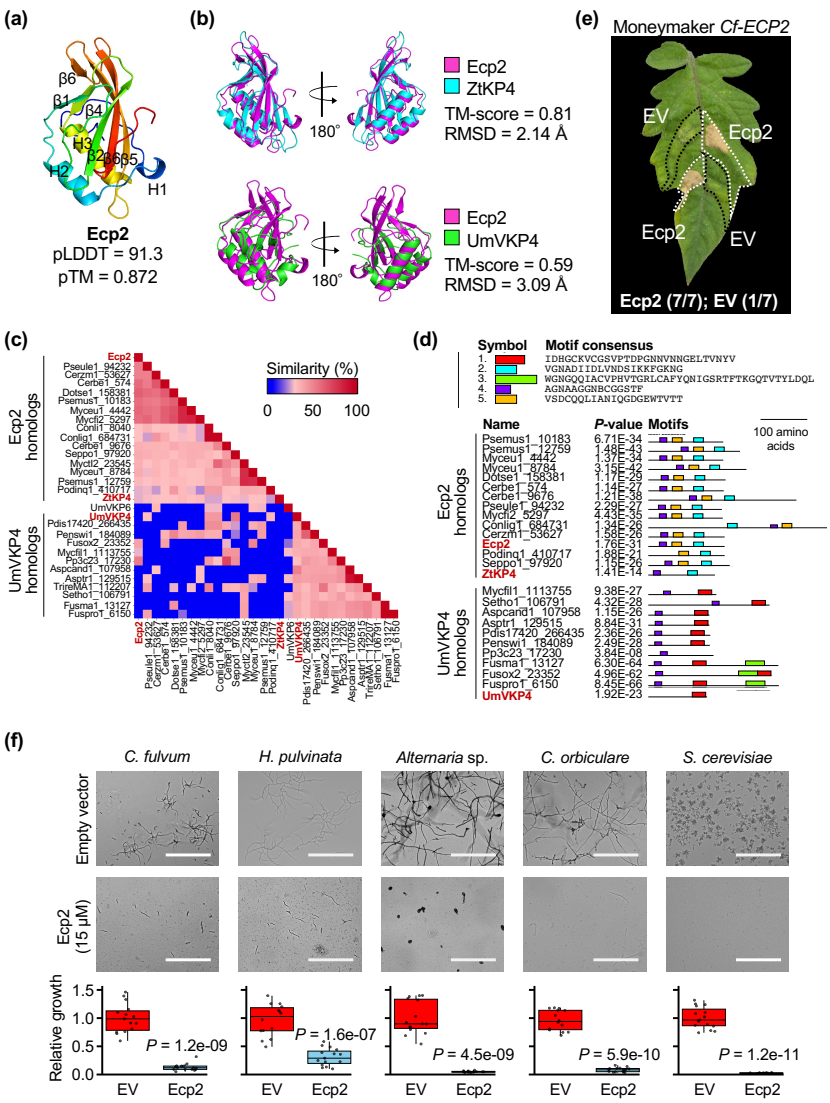

Fig. 6. Sequence dissimilarity and structural similarity between *Cladosporium fulvum* effector Ecp2 and killer toxin KP4 proteins. (a) Predicted 3D structure of Ecp2 generated using AlphaFold2. The color spectrum from blue to red indicates the N- to C-terminal positions of residues. (b) Structural comparison of Ecp2 with ZtKP4 and UmVKP4 proteins. The superposition of the aligned proteins was evaluated using TM-align, and the TM-score and RMSD values are shown. (c) Heatmap showing sequence similarity among Ecp2, ZtKP4, and UmVKP4 proteins as identified by BLASTp analysis. (d) Conserved motifs of the proteins identified by MEME motif analysis. (e) Representative tomato leaf from 4-week-old tomato plant carrying the *Cf-ECP2* resistance gene at 6 days after infiltration with purified Ecp2 protein produced by *Escherichia coli*. White dotted outline: area infiltrated with infiltrated with 1 μM Ecp2; black dotted outline: infiltrated with control protein purified from *E. coli* harboring an empty vector (EV). Numbers in parentheses indicate the number of leaves with a hypersensitive response (HR) relative to the number of total leaves. (f) *In vitro*

555 antifungal activity of Ecp2 against *C. fulvum*, *H. pulvinata*, *Alternaria* sp., *Colletotrichum*
556 *orbiculare*, and *Saccharomyces cerevisiae*. Spores were cultured on 5% potato dextrose agar
557 with or without Ecp2. Relative hyphal length was determined 4 days after treatment. Bars =
558 250 µm. Significant differences between EV and Ecp2 treatments were assessed using
559 Student's t-test, and *p*-values are indicated.
560
561 To explore the evolutionary relationships among these KP4-like proteins, we searched
562 for homologs of Ecp2, ZtKP4, and UmVKP4. Nineteen Ecp2 homologs were identified
563 across three fungal classes, while only one ZtKP4 homolog was detected in *Zymoseptoria*
564 *tritici* (syn. *Mycosphaerella graminicola*) (Table **S9**). A total of 188 UmVKP4 homologs
565 were found in 10 classes. Based on sequence similarity, these proteins clustered into two
566 groups; Ecp2 and ZtKP4 were placed in the same clade (Fig. **6c**). Motif analysis revealed
567 distinct conserved amino acid motifs in each group, and UmVKP4 group lacked an Hce2
568 domain (Fig. **6d**). While Ecp2 and ZtKP4 shared two conserved disulfide bonds, UmVKP4
569 had five, suggesting differences in structural stability and folding despite their shared overall
570 architecture (Fig. **S7b**). These results indicated that Ecp2 and UmVKP4 protein groups likely
571 originated from two distinct evolutionary lineages.
572 Given that Ecp2 is structurally and phylogenetically close to ZtKP4, which has
573 antifungal activity (de Guillen *et al*., 2024), we investigated the antifungal potential of Ecp2.
574 Infiltration of *Cf-ECP2* tomato leaves with recombinant Ecp2 (Fig. **S7c**) triggered a specific
575 HR (Fig. **6e**). At the high concentrations used, the active Ecp2 protein significantly inhibited
576 hyphal growth in diverse fungi: *C. fulvum*, *H. pulvinata*, *Alternaria* sp. isolated from tomato
577 fruits, the plant pathogen *Colletotrichum orbiculare* and the yeast *Saccharomyces cerevisiae*
578 (Fig. **6f**). Together, these results demonstrated that Ecp2 has a dual role: inducing *Cf-ECP2*-
579 mediated immunity in plant while inhibiting fungal growth. *H. pulvinata* exhibited
580 marginally higher resistance than the other tested fungi and yeast to Ecp2.
581
582 **Enrichment analysis of DEGs and KEGG pathways in tomato plants**
583 We also analyzed differential gene expression in tomato leaves inoculated with *C. fulvum*
584 and inoculated with *C. fulvum* followed by *H. pulvinata*, each compared with uninoculated
585 control leaves (Fig. **1a**). Infection by *C. fulvum* alone led to 3,231 upregulated and 4,980
586 downregulated genes, whereas in the presence of *H. pulvinata* (*on planta Cf/Hp*), 3,465 genes
587 were upregulated and 5,679 downregulated (Fig. **7a**). Among these, 1,619 up- and 2,153
588 downregulated genes were uniquely responsive to *H. pulvinata*, mapping to 35 and 33

589 enriched KEGG pathways, respectively (Fig. **7b**). Pathways associated with plant–pathogen
590 interaction, phytoalexin biosynthesis (stilbenoid, diarylheptanoid and gingerol), biosynthesis
591 of unsaturated fatty acids, other secondary metabolites, phenylpropanoid biosynthesis and
592 plant hormone signal transduction were induced when *H. pulvinata* parasitized *C. fulvum* on
593 leaves (Fig. **7b**). Genes encoding calcium-dependent protein kinases, PR1, RIN4, MAP
594 kinase, WRKY22 and defensins were highly expressed (Fig. **S8a**; Table **S10**). These results
595 indicated that *H. pulvinata* triggers plant immunity during parasitisation of *C. fulvum* on
596 tomato leaves. In contrast, pathways associated with photosynthesis antenna proteins and
597 porphyrin metabolism, which is involved in chlorophyll biosynthesis, were upregulated
598 during infection by *C. fulvum* alone, but significantly downregulated when parasitized by *H.*
599 *pulvinata* (Fig. **7b**; Fig. **S8b** and **c**), indicating that *H. pulvinata* triggered pronounced plant
600 resistance responses during parasitisation of *C. fulvum*.

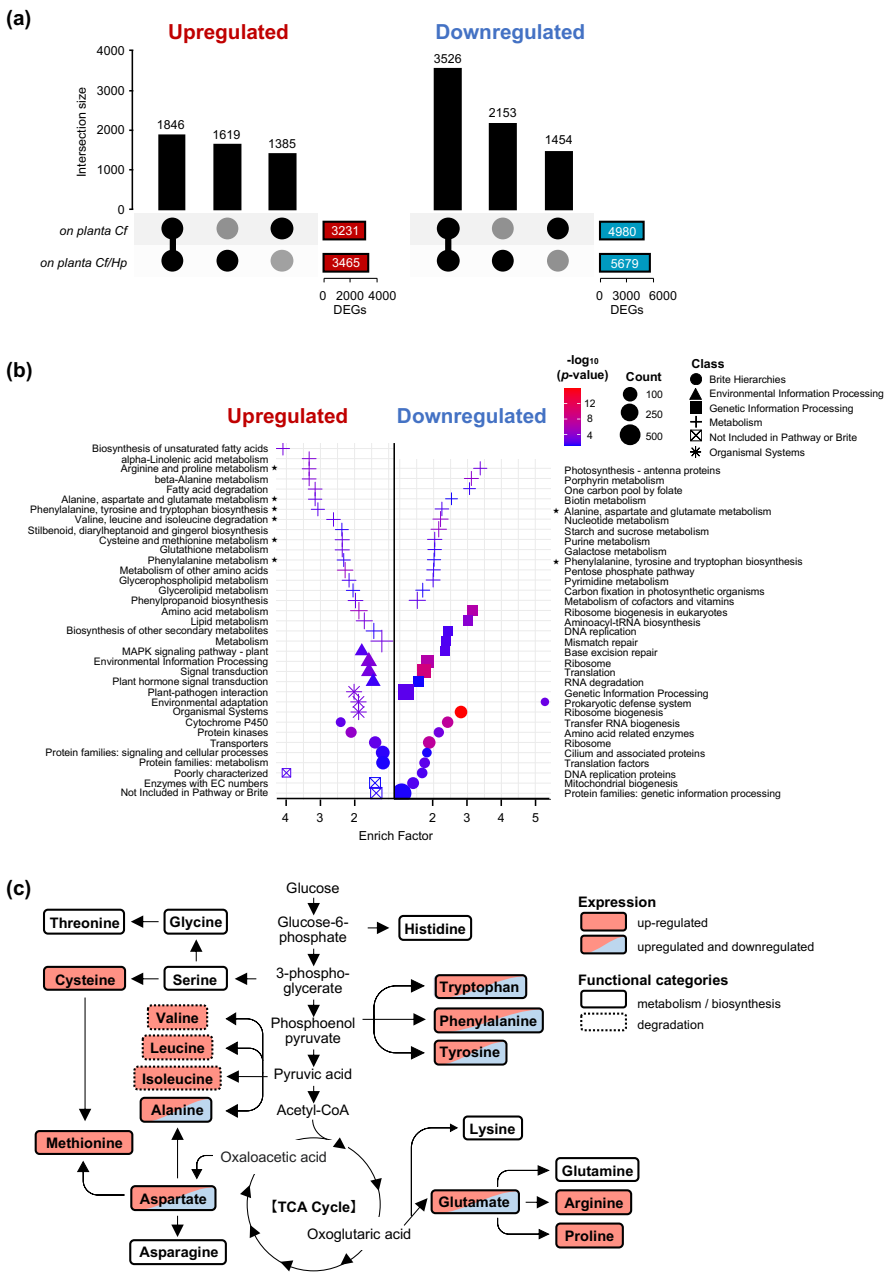

Fig. 7. Differentially expressed genes (DEGs) and enriched KEGG pathways in tomato plants. (a) UpSet plot of DEGs in the *on planta Cf* and *on planta Cf/Hp* conditions (see Fig. 1a). Healthy leaves were used as a control. Connected dots indicate shared DEGs; Black single dots represent condition-specific DEGs. Vertical bars show the number of up- and downregulated genes; colored horizontal bars indicate the total number of DEGs detected in each interaction. (b) Bubble plot of KEGG pathway enrichment analysis based on the 1,619 and 2,153 DEGs shown in (a). Keys: color of symbols indicates significance level of enrichment (–log adjusted *P*); size of symbol indicates the number of enriched DEGs in each pathway; the symbol indicates the functional class of the enriched DEGs. Stars indicate

611 pathways highlighted in (c). (c) KEGG pathways involved in amino acid biosynthesis in
612 tomato.
613 Strikingly, 13 amino acid biosynthesis and metabolism pathways were strongly activated
614 in the *on planta Cf/Hp* condition (Fig. **7b** and **c**). Although amino acid metabolism was
615 broadly repressed in both *C. fulvum* and *H. pulvinata* during mycoparasitism (Fig. **2b**; Fig.
616 **4b**), it was upregulated in tomato (Fig. **7b** and **c**). The pronounced activation of amino acid
617 biosynthesis pathways in tomato suggests that the plant supplies amino acids to both the
618 pathogen *C. fulvum* and its mycoparasite *H. pulvinata* during the tritrophic interaction.
619

620 **DISCUSSION**

621 In this study, we analyzed gene expression in tomato plants, the phytopathogenic fungus *C.*
622 *fulvum*, and its mycoparasite *H. pulvinata* alone or during their bitrophic and tritrophic
623 interaction to capture coordinated and distinct responses. We thus discovered previously
624 unrecognized aspects of molecular crosstalk and revealed how the transcriptome of each
625 organism was dynamically reprogrammed during these interactions.
626

627 **Evolutionary and functional insights into an atypical NLP in the biocontrol**
628 **mycoparasite *H. pulvinata***

629 The identification of 165 secreted small proteins upregulated during mycoparasitism
630 highlights the central role of the secretome of *H. pulvinata*. Among them, HpNlp1, an
631 atypical NLP, lacked both necrosis-inducing activity or RLP23 receptor-mediated response in
632 plants, unlike canonical NLPs such as PsojNIP (Qutob *et al*., 2006; Böhm *et al*., 2014; Oome
633 *et al*., 2014). Instead, HpNlp1 accumulated antifungal substances in the apoplast and
634 inhibited spore germination of *C. fulvum*. Although *H. pulvinata* cannot grow independently
635 on tomato leaves (Iida *et al*., 2018), it follows the hyphae of *C. fulvum* that enter the stomata
636 of tomato leaves (Fig. **S1b**), indicating that the two fungi co-occur in the tomato apoplast.
637 Furthermore, the functional divergence of the NLPs between the pathogen and mycoparasite
638 indicates the evolutionary plasticity of NLP family. Despite its structural similarity to
639 PsojNIP, HpNlp1 has distinct biological functions, suggesting that subtle amino acid
640 modifications can drive functional divergence within the NLP family. If *H. pulvinata* induced
641 a strong necrotic or immune response in tomato, the host fungus *C. fulvum* would decline,
642 limiting its own nutrient supply. Therefore, the high upregulation of a noncytotoxic NLP such
643 as HpNlp1 during mycoparasitism is evolutionarily reasonable. Notably, the *HpNLP1* gene
644 was expressed in *H. pulvinata* when parasiting its host *on planta* and *in vitro*, suggesting that

645 it recognizes *C. fulvum* itself rather than plant-derived signals. Although HpNlp1 did not
646 directly inhibit *C. fulvum* growth, it indirectly promoted the accumulation of antifungal
647 metabolites, suggesting coevolution of *H. pulvinata* with not only its fungal host *C. fulvum*
648 but also tomato plants.
649 KEGG enrichment analysis indicated that *H. pulvinata* activated multiple secondary
650 metabolic pathways, particularly those related to terpenoids, polyketides, steroids and *DPH*
651 biosynthetic gene cluster, during mycoparasitism. These findings agree with previous
652 findings that *H. pulvinata* produces 13-deoxyformenone, an eremophilane-type
653 sesquiterpenoid, which is fungistatic to *C. fulvum* (Maeda *et al*., 2025). The production of
654 antifungal substances triggered by HpNlp1 in the tomato apoplast was correlated with the
655 induction of genes encoding defensins and phytoalexins, which were expressed only when *C.*
656 *fulvum* was parasitized by *H. pulvinata* on tomato leaves. Given that similar noncytotoxic
657 NLPs from the biocontrol oomycete *Pythium oligandrum* also induce plant defensins (Yang
658 *et al*., 2022), HpNlp1 may represent a conserved mechanism among biocontrol agents that
659 modulate plant immunity without causing cell death. *H. pulvinata* may employ a two-tiered
660 strategy to preserve the spores of its host fungus *C. fulvum*, combining a direct antifungal
661 sesquiterpenoid with an indirect, noncytotoxic protein, HpNlp1.
662
663 **Ecp2 effector as a novel antifungal protein in the pathogen *C. fulvum***
664 KP4 family proteins, broadly conserved in phytopathogenic fungi, are antifungal but do not
665 interact with the plant. For instance, *U. maydis* UmVKP4 suppresses the growth of
666 susceptible strains of the same species by inhibiting calcium-dependent pathways that
667 regulate the cell cycle and morphogenesis (Gu *et al*., 1995; Gage *et al*., 2002). *Z. tritici*
668 ZtKP4 has fungicidal activity even against itself (de Guillen *et al*., 2024). Our structural
669 modeling showed that *C. fulvum* Ecp2 shared similarity with KP4 proteins and had broad-
670 spectrum antifungal activity ranging from filamentous fungi to yeast, including self-inhibition
671 similar to that of ZtKP4. The β1–β2 loop in Ecp2 should functionally correspond to the β3–
672 β4 loop of UmVKP4, which mediates interactions with intracellular proteins (Gu *et al*.,
673 1995). However, Ecp2 lacked the key lysine residue (Lys42) that UmVKP4 requires for full
674 antifungal activity (Gage *et al*., 2001), suggesting a similar mechanism underlying antifungal
675 action but involving an alternative molecular interface. During the arms race between tomato
676 and *C. fulvum*, a KP4-like antifungal protein may have been diverted to Ecp2 effector.
677 However, the structural basis underlying *CfECP2*-mediated immune recognition and how

678 Ecp2 acquired the dual ability to interact with both fungal and plant targets remain
679 unresolved.
680 Ecp2 was strongly expressed even during *in vitro* mycoparasitism, suggesting a dual role
681 as both a virulence factor against plants and an antifungal protein in microbial competition.
682 Similar dual functionality is seen in the root endophyte *Serendipita* spp., where a chitinase
683 encoding effector is induced during both plant colonization and microbial interaction
684 (Eichfeld *et al*., 2024). The vascular wilt fungus *Verticillium dahliae* secretes antimicrobial
685 effectors such as VdAve1 and VdAMP2 to gain an ecological advantage in the soil biome
686 (Snelders *et al*., 2020). The soil-borne white root rot pathogen *Rosellinia necatrix*, which is
687 phylogenetically related to *V. dahliae*, secretes antimicrobial effector proteins during host
688 plant colonization (Chavarro-Carrero *et al*., 2024). While the rhizosphere harbors highly
689 diverse and competitive microbial communities, the diversity of the microbial community in
690 the endosphere such as the apoplastic space is generally relatively low (Snelders *et al*., 2022)
691 because colonization of the apoplast is typically restricted to specialized microbes that can
692 secrete effectors to suppress host immunity (Rocafort *et al*., 2020). In fact, despite previous
693 predictions that some apoplastic effectors produced by *C. fulvum* may have antimicrobial
694 activity, no direct evidence had been found so far (Mesarich *et al*., 2018). Our finding
695 indicates the potential for *C. fulvum* not only to utilize effectors for efficient colonization of
696 tomato leaves but also to compete with/inhibit other microbes in the endosphere and
697 phyllosphere. Although *H. pulvinata* was moderately tolerant of Ecp2, the molecular basis for
698 this tolerance during mycoparasitism remains unclear.
699 The Hce2 (Homologs of *C. fulvum* Ecp2) superfamily is widely conserved across the
700 *Ascomycota* and *Basidiomycota*, suggesting that its origin predates the divergence of the
701 *Dikarya* lineage (Stergiopoulos *et al*., 2012). In contrast, *U. maydis* UmVKP4, which shares
702 structural similarity with Ecp2, lacks the Hce2 domain and shared sequence motifs, and
703 differs in the number of disulfide bonds (Fig. **S7b**). These findings suggest that UmVKP4
704 represents a case of convergent evolution, resulting in structural resemblance to Ecp2 and
705 ZtKP4. Molecular evolutionary analyses suggest that the amino acid substitution underlying
706 Hce2 function diversification was fixed early in evolution (Stergiopoulos *et al*., 2012).
707 Ancestral Hce2 proteins may initially act as antimicrobial factors to provide competitive
708 advantages in microbe-rich habitats, and have been co-opted as an effector to inhibit plant
709 immunity. Mutations in effector genes that allow *C. fulvum* to evade *Cf* resistance in plants
710 may increase its susceptibility to antagonistic microbes such as *H. pulvinata*. This hypothesis

711 suggests that mycoparasitic biocontrol agents can circumvent the classical arms race between
712 plant and pathogen, providing a sustainable disease management.
713
714 **Potential metabolic trade-offs in amino acid pathways between fungi and tomato plants**
715 The physiological changes found in tomato plants highlight the dynamic interplay between
716 microbial interplay and plant defense responses. The expression of genes in multiple amino
717 acid biosynthetic pathways were enhanced only when *H. pulvinata* parasitized *C. fulvum* on
718 tomato leaves. Amino acids are key mediators of plant–microbe interactions, functioning as
719 signaling molecules that activate defense and as nutritional sources that are exploited by
720 pathogens (Moormann *et al*., 2022; Tünnermann *et al*., 2022). Indeed, infection by *C. fulvum*
721 leads to the accumulation of free amino acids in the apoplast (Solomon & Oliver, 2001).
722 Because the acquisition of plant-derived amino acids is energetically advantageous to
723 microbes, many plant pathogens modulate expression of genes encoding amino acid
724 transporters to optimize uptake (Sonawala *et al*., 2018). Thus, the regulation of amino acid
725 assimilation and transport in plants can be a decisive factor shaping the outcome of plant–
726 pathogen interactions.
727 In contrast, amino acid biosynthetic pathways in *H. pulvinata* and *C. fulvum* were
728 downregulated under mycoparasitic conditions, suggesting that tomato-derived amino acids
729 could be shared or sequentially utilized by these fungi (Fig. **8**). In this metabolic trade-off,
730 tomato plants might invest in amino acids that benefit *H. pulvinata*, while receiving
731 biocontrol protection in return. Although amino acids are fundamental primary metabolites
732 during fungal vegetative growth, the metabolic profile of *H. pulvinata*, which exhibited
733 vigorous hyphal growth during mycoparasitism, deviated from this conventional paradigm.
734 Because *H. pulvinata* parasitizes *C. fulvum*, it likely becomes the recipient of these plant-
735 derived nutrients via its host *C. fulvum*, forming a potential metabolic trade-off in the
736 tritrophic interaction. In this context, the activation of amino acid biosynthesis in tomato may
737 provide a nutritional foundation that ultimately supports colonization and biocontrol activity
738 by *H. pulvinata*. Although *C. fulvum* may also acquire amino acids from plants, these
739 resources are likely reallocated to *H. pulvinata*, the ultimate beneficiary of the tritrophic
740 interaction. Similar strategies have been reported for the biocontrol fungus *Pseudozyma*
741 *flocculosa,* active against powdery mildews, which transiently suppresses photosynthesis to
742 promote amino acid release (Laur *et al*., 2018). The mycoparasitic fungus *Trichoderma*
743 *erinaceum* exploits environmental amino acids to enhance the synthesis of antifungal
744 secondary metabolites derived from amino acids (Guo *et al*., 2020). Together, these results

745 suggested that shifts in amino acid metabolism enable *H. pulvinata* to harness pathogen-
746 induced plant responses to its own benefit.
747

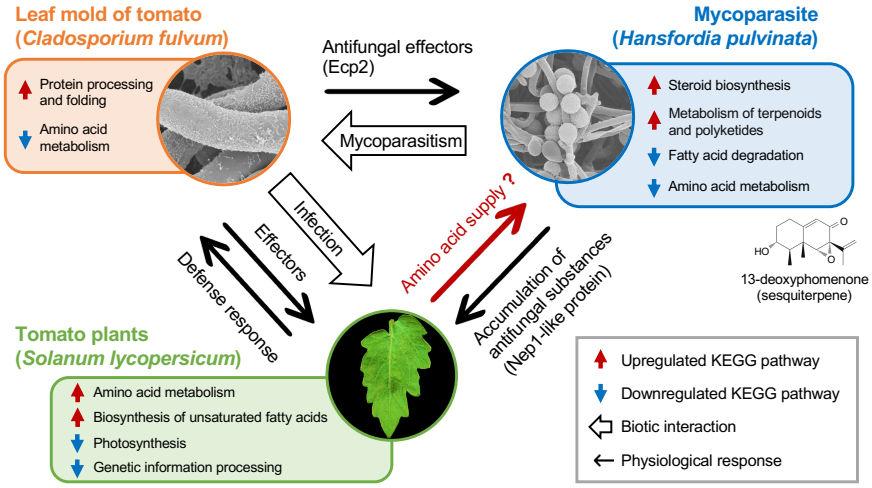

748
749 **Fig. 8. Overview of the tritrophic interaction between tomato plants, the pathogen**
750 ***Cladosporium fulvum*, and its mycoparasite *Hansfordia pulvinata*.** *C. fulvum* secretes
751 effector proteins that function as virulence factors in susceptible tomato cultivars and
752 antifungal proteins active against other fungi, but act as avirulence factors upon recognition
753 by *Cf*- containing resistant cultivars. *H. pulvinata* parasitizes *C. fulvum* and induces the
754 production of apoplastic antifungal substances in tomato plants via the Nep1-like protein
755 HpNlp1. *H. pulvinata* also activates the biosynthesis of the antifungal sesquiterpene 13-
756 deoxyphomenone during mycoparasitism. Other plant defense responses support this
757 biocontrol effect. Pathways related to amino acid biosynthesis in the three organisms suggest
758 that nutrients from the plant are supplied to *H. pulvinata*.
759
760 **Mycoparasitism by *H. pulvinata* modulates plant immunity and pathogen growth**
761 In conclusion, the mycoparasite *H. pulvinata* actively reprogrammes gene expression and
762 physiological responses in the pathogen *C. fulvum* and its tomato host to establish a stable
763 tritrophic interaction (Fig. **8**). *H. pulvinata* induced expression of the 13-deoxyphomenone
764 biosynthetic gene cluster in tomato plants; antimicrobial substances accumulated in the
765 apoplast and directly suppressed *C. fulvum*, thus enhancing plant resistance. In turn, *C.*
766 *fulvum* secretes effectors such as Ecp2 that exhibites roles in both fungal competition and
767 plant immunity. During the tritrophic interaction in tomato, amino acid metabolism and
768 defense response pathways are reprogrammed, orchestrating distinct strategies against
769 beneficial and pathogenic microbes. Collectively, these findings underscore the dynamic

interplay in plant–pathogen–mycoparasite interactions, demonstrating that *H. pulvinata* simultaneously strengthens tomato immunity and represses *C. fulvum* virulence via direct antagonism and modulation of plant metabolic pathways.

ACKNOWLEDGEMENTS

This work was supported by a Grant-in-Aid for Scientific Research from JSPS (20H02993 and 24K08919) and the Research and Implementation Promotion Program through Open Innovation Grants (JPJ011937) from the Project of the Bio-oriented Technology Research Advancement Institution (BRAIN) (Y. Iida). We are grateful to K. Ikeda for providing fungal strains, M.H.A.J. Joosten for *Cf-ECP2* tomato seeds, D. Takemoto for the *psojNIP* gene, F. Takken for pSfinx, and Y. Kubo for the *C. orbiculare* strain. We thank Y. Kubo, M.Z. Fanani and S. Kodama for valuable suggestions, C. Tanaka for laboratory management, P.J.G.M. de Wit for critical reading of the manuscript.

COMPETING INTERESTS

The authors declare that they have no commercial or financial relationships that could be construed as a potential conflict of interest.

AUTHOR CONTRIBUTIONS

YI designed the study and managed the research funds. KM, HS and TaS performed RNA-seq and analyzed the data. KM, MK, MO, and TK analyzed NLPs. ToS conducted electron microscopy and EI developed a microscopic observation protocol. KM and KS studied the Ecp2 protein. KM and YI wrote the manuscript. All authors reviewed and approved the final version.

DATA AVAILABILITY

Genomic sequences for *C. fulvum* strain Race5_Kim and *H. pulvinata* strain 414-3 are available as accessions PRJNA565804 and PRJDB8178 at NCBI BioProject, respectively (Sushida *et al*., 2019; Zaccaron & Stergiopoulos, 2024). Tomato genome data were obtained from the Solanaceae Genomics Network (Hosmani *et al*., 2019). Additional genomes are accessible via JGI MycoCosm (mycocosm.jgi.doe.gov) and the DDBJ/EMBL/GenBank repository (www.ncbi.nlm.nih.gov). Custom scripts and supporting datasets were deposited at Figshare (doi.org/10.6084/m9.figshare.30265009).

REFERENCES

Bailey TL, Johnson J, Grant CE, Noble WS. 2015. The MEME Suite. *Nucleic Acids Research*. 2015 Jul 1;43(W1):W39-49. doi: 10.1093/nar/gkv416. Epub 2015 May 7. PMID: 25953851; PMCID: PMC4489269.

Berg S, Kutra D, Kroeger T, Straehle CN, Kausler BX, Haubold C, Schiegg M, Ales J, Beier T, Rudy M, et al. 2019. ilastik: interactive machine learning for (bio)image analysis. *Nature Methods*. 2019 Dec;16(12):1226-1232. doi: 10.1038/s41592-019-0582-9. Epub 2019 Sep 30. PMID: 31570887.

Blin K, Shaw S, Augustijn HE, Reitz ZL, Biermann F, Alanjary M, Fetter A, Terlouw BR, Metcalf WW, Helfrich EJN, et al. 2023. antiSMASH 7.0: new and improved predictions for detection, regulation, chemical structures and visualisation. *Nucleic Acids Research*. 2023 Jul 5;51(W1):W46-W50. doi: 10.1093/nar/gkad344. PMID: 37140036; PMCID: PMC10320115.

Böhm H, Albert I, Oome S, Raaymakers TM, Van den Ackerveken G, Nürnberger T. 2014. A conserved peptide pattern from a widespread microbial virulence factor triggers pattern-induced immunity in *Arabidopsis*. *PLOS Pathogens*. 2014 Nov 6;10(11):e1004491. doi: 10.1371/journal.ppat.1004491. PMID: 25375108; PMCID: PMC4223075.

Bolger AM, Lohse M, Usadel B. 2014. Trimmomatic: a flexible trimmer for Illumina sequence data. *Bioinformatics*. 2014 Aug 1;30(15):2114-20. doi: 10.1093/bioinformatics/btu170. Epub 2014 Apr 1. PMID: 24695404; PMCID: PMC4103590.

Capella-Gutiérrez S, Silla-Martínez JM, Gabaldón T. 2009. trimAl: a tool for automated alignment trimming in large-scale phylogenetic analyses. *Bioinformatics*. Aug 1;25(15):1972-3. doi: 10.1093/bioinformatics/btp348. Epub 2009 Jun 8. PMID: 19505945; PMCID: PMC2712344.

Chaillot J, Tebbji F, Remmal A, Boone C, Brown GW, Bellaoui M, Sellam A. 2015. The Monoterpene Carvacrol Generates Endoplasmic Reticulum Stress in the Pathogenic Fungus *Candida albicans*. *Antimicrobial Agents and Chemotherapy*. 2015 Aug;59(8):4584-92. doi: 10.1128/AAC.00551-15. Epub 2015 May 26. PMID: 26014932; PMCID: PMC4505245.

Chavarro-Carrero EA, Snelders NC, Torres DE, Kraege A, López-Moral A, Petti GC, Punt W, Wieneke J, García-Velasco R, López-Herrera CJ, et al. 2024. The soil-borne white root rot pathogen *Rosellinia necatrix* expresses antimicrobial proteins during host

838 colonization. *PLOS Pathogens*. 2024 Jan 18;20(1):e1011866. doi:
839 10.1371/journal.ppat.1011866. PMID: 38236788; PMCID: PMC10796067.
840 **Chen C, Wu Y, Li J, Wang X, Zeng Z, Xu J, Liu Y, Feng J, Chen H, He Y,** et al. 2023.
841 TBtools-II: A "one for all, all for one" bioinformatics platform for biological big-data
842 mining. *Molecular Plant*. 2023 Nov 6;16(11):1733-1742. doi:
843 10.1016/j.molp.2023.09.010. Epub 2023 Sep 22. PMID: 37740491.
844 **Eichfeld R, Mahdi LK, De Quattro C, Armbruster L, Endeshaw AB, Miyauchi S,**
845 **Hellmann MJ, Cord-Landwehr S, Peterson D, Singan V,** et al. 2024. Transcriptomics
846 reveal a mechanism of niche defense: two beneficial root endophytes deploy an
847 antimicrobial GH18-CBM5 chitinase to protect their hosts. *New Phytologist*. 2024
848 Nov;244(3):980-996. doi: 10.1111/nph.20080. Epub 2024 Sep 3. PMID: 39224928.
849 **Emms DM, Kelly S.** 2019. OrthoFinder: phylogenetic orthology inference for comparative
850 genomics. *Genome Biology*. 2019 Nov 14;20(1):238. doi: 10.1186/s13059-019-1832-y.
851 PMID: 31727128; PMCID: PMC6857279.
852 **Gage MJ, Bruenn J, Fischer M, Sanders D, Smith TJ.** 2001. KP4 fungal toxin inhibits
853 growth in *Ustilago maydis* by blocking calcium uptake. *Molecular Microbiology*. 2001
854 Aug;41(4):775-85. doi: 10.1046/j.1365-2958.2001.02554.x. PMID: 11532143.
855 **Gage MJ, Rane SG, Hockerman GH, Smith TJ**. 2002. The virally encoded fungal toxin
856 KP4 specifically blocks L-type voltage-gated calcium channels. *Molecular*
857 *Pharmacology*. 2002 Apr;61(4):936-44. doi: 10.1124/mol.61.4.936. PMID: 11901234.
858 **Gene Ontology Consortium; Aleksander SA, Balhoff J, Carbon S, Cherry JM, Drabkin**
859 **HJ, Ebert D, Feuermann M, Gaudet P, Harris NL**, et al. 2023. The Gene Ontology
860 knowledgebase in 2023. *Genetics*. 2023 May 4;224(1):iyad031. doi:
861 10.1093/genetics/iyad031. PMID: 36866529; PMCID: PMC10158837.
862 **Gíslason MH, Nielsen H, Almagro Armenteros JJ, Johansen AR.** 2021. Prediction of
863 GPI-anchored proteins with pointer neural networks. *Current Research in Biotechnology*.
864 2021;3:6-13. doi:10.1016/j.crbiot.2021.01.001.
865 **Griffiths S, Mesarich CH, Overdijk EJR, Saccomanno B, de Wit PJGM, Collemare J.**
866 2018. Down-regulation of cladofulvin biosynthesis is required for biotrophic growth of
867 *Cladosporium fulvum* on tomato. *Molecular Plant Pathology*. 2018 Feb;19(2):369-380.
868 doi: 10.1111/mpp.12527. Epub 2017 Feb 6. PMID: 27997759; PMCID: PMC6638085.
869 **Gu F, Khimani A, Rane SG, Flurkey WH, Bozarth RF, Smith TJ.** 1995. Structure and
870 function of a virally encoded fungal toxin from *Ustilago maydis*: a fungal and

mammalian Ca2+ channel inhibitor. *Structure*. 1995 Aug 15;3(8):805-14. doi: 10.1016/s0969-2126(01)00215-5. PMID: 7582897.

de Guillen K, Mammri L, Gracy J, Padilla A, Barthe P, Hoh F, Lahfa M, Rouffet J, Petit-Houdenot Y, Kroj T, et al. 2024. *Zymoseptoria tritici* effectors structurally related to killer proteins UmV-KP4 and UmV-KP6 are toxic to fungi, and define extended protein families in fungi. *bioRxiv*. 2024 Oct 14:2024.10.14.618152. doi:10.1101/2024.10.14.618152.

Guo YW, Gong BQ, Yuan J, Li HJ, Mahmud T, Huang Y, Li JF, Yang DP, Lan WJ. 2020. l-Phenylalanine Alters the Privileged Secondary Metabolite Production in the Marine-Derived Fungus T*richoderma erinaceum* F1-1. *Journal of Natural Products*. 2020 Jan 24;83(1):79-87. doi: 10.1021/acs.jnatprod.9b00710. Epub 2019 Dec 30. PMID: 31886665.

Holm L. 2022. Dali server: structural unification of protein families. *Nucleic Acids Research*. 2022 Jul 5;50(W1):W210-W215. doi: 10.1093/nar/gkac387. PMID: 35610055; PMCID: PMC9252788.

Hosmani PS, Flores-Gonzalez M, van de Geest H, Maumus F, Bakker LV, Schijlen E, van Haarst J, Cordewener J, Sanchez-Perez G, Peters S, et al. 2019. An improved de novo assembly and annotation of the tomato reference genome using single-molecule sequencing, Hi-C proximity ligation and optical maps. *bioRxiv*. 2019;767764. doi:10.1101/767764

Iida Y, Ikeda K, Sakai H, Nakagawa H, Nishi O, Higashi Y. 2018. Evaluation of the potential biocontrol activity of *Dicyma pulvinata* against *Cladosporium fulvum*, the causal agent of tomato leaf mold. *Plant Pathology*. 2018;67(9):1883–1890. doi:10.1111/ppa.12916.

Iida Y, van 't Hof P, Beenen H, Mesarich C, Kubota M, Stergiopoulos I, Mehrabi R, Notsu A, Fujiwara K, Bahkali A, et al. 2015. Novel Mutations Detected in Avirulence Genes Overcoming Tomato *Cf* Resistance Genes in Isolates of a Japanese Population of *Cladosporium fulvum*. *PLoS One*. 2015 Apr 22;10(4):e0123271. doi: 10.1371/journal.pone.0123271. PMID: 25902074; PMCID: PMC4406682.

de Jonge R, van Esse HP, Kombrink A, Shinya T, Desaki Y, Bours R, van der Krol S, Shibuya N, Joosten MH, Thomma BP. 2010. Conserved fungal LysM effector Ecp6 prevents chitin-triggered immunity in plants. *Science*. 2010 Aug 20;329(5994):953-5. doi: 10.1126/science.1190859. PMID: 20724636.

904 **Joosten MH.** 2012. Isolation of apoplastic fluid from leaf tissue by the vacuum infiltration-
905 centrifugation technique. *Methods in Molecular Biology*. 2012;835:603-10. doi:
906 10.1007/978-1-61779-501-5_38. PMID: 22183681.
907 **Kanehisa M, Furumichi M, Sato Y, Matsuura Y, Ishiguro-Watanabe M.** 2025. KEGG:
908 biological systems database as a model of the real world. *Nucleic Acids Research*. 2025
909 Jan 6;53(D1):D672-D677. doi: 10.1093/nar/gkae909. PMID: 39417505; PMCID:
910 PMC11701520.
911 **Katoh K., Standley DM.** 2013. MAFFT multiple sequence alignment software version 7:
912 improvements in performance and usability. *Molecular biology and*
913 *evolution*. Apr;30(4):772-80. doi: 10.1093/molbev/mst010. Epub 2013 Jan 16. PMID:
914 23329690; PMCID: PMC3603318.
915 **Kim D, Paggi JM, Park C, Bennett C, Salzberg SL.** 2019. Graph-based genome alignment
916 and genotyping with HISAT2 and HISAT-genotype. *Nature Biotechnology*. 2019
917 Aug;37(8):907-915. doi: 10.1038/s41587-019-0201-4. Epub 2019 Aug 2. PMID:
918 31375807; PMCID: PMC7605509.
919 **de Kock MJ, Iskandar HM, Brandwagt BF, Laugé R, de Wit PJGM, Lindhout P.** 2004.
920 Recognition of *Cladosporium fulvum* Ecp2 elicitor by non-host *Nicotiana* spp. is
921 mediated by a single dominant gene that is not homologous to known *Cf*-genes.
922 *Molecular Plant Pathology*. 2004 Sep 1;5(5):397-408. doi: 10.1111/j.1364-
923 3703.2004.00239.x. PMID: 20565616.
924 **Kourelis J, Malik S, Mattinson O, Krauter S, Kahlon PS, Paulus JK, van der Hoorn**
925 **RAL.** 2020. Evolution of a guarded decoy protease and its receptor in solanaceous
926 plants. *Nature Communications*. 2020 Sep 2;11(1):4393. doi: 10.1038/s41467-020-
927 18069-5. Erratum in: *Nature Communications*. 2024 Mar 13;15(1):2278. doi:
928 10.1038/s41467-024-46611-2. PMID: 32879321; PMCID: PMC7468133.
929 **Laur J, Ramakrishnan GB, Labbé C, Lefebvre F, Spanu PD, Bélanger RR.** 2018.
930 Effectors involved in fungal-fungal interaction lead to a rare phenomenon of
931 hyperbiotrophy in the tritrophic system biocontrol agent-powdery mildew-plant. *New*
932 *Phytologist*. 2018 Jan;217(2):713-725. doi: 10.1111/nph.14851. Epub 2017 Oct 18.
933 PMID: 29044534; PMCID: PMC6079639.
934 **Li H, Handsaker B, Wysoker A, Fennell T, Ruan J, Homer N, Marth G, Abecasis G,**
935 **Durbin R; 1000 Genome Project Data Processing Subgroup**. 2009. The Sequence
936 Alignment/Map format and SAMtools. *Bioinformatics*. 2009 Aug 15;25(16):2078-9. doi:

937 10.1093/bioinformatics/btp352. Epub 2009 Jun 8. PMID: 19505943; PMCID:
938 PMC2723002.
939 **Love MI, Huber W, Anders S**. 2014. Moderated estimation of fold change and dispersion
940 for RNA-seq data with DESeq2. *Genome Biology*. 2014;15(12):550. doi:
941 10.1186/s13059-014-0550-8. PMID: 25516281; PMCID: PMC4302049.
942 **Luderer R, Takken FL, de Wit PJGM, Joosten MH.** 2002. *Cladosporium fulvum*
943 overcomes *Cf-2*-mediated resistance by producing truncated AVR2 elicitor proteins.
944 Molecular *Microbiology*. 2002 Aug;45(3):875-84. doi: 10.1046/j.1365-
945 2958.2002.03060.x. PMID: 12139631.
946 **Ma L, Lukasik E, Gawehns F, Takken FL.** 2012. The use of agroinfiltration for transient
947 expression of plant resistance and fungal effector proteins in *Nicotiana benthamiana*
948 leaves. *Methods in Molecular Biology*. 2012;835:61-74. doi: 10.1007/978-1-61779-501-
949 5_4. PMID: 22183647.
950 **Madeira F, Madhusoodanan N, Lee J, Eusebi A, Niewielska A, Tivey ARN, Lopez R,**
951 **Butcher S.** 2024. The EMBL-EBI Job Dispatcher sequence analysis tools framework in
952 2024. *Nucleic Acids Research*. 2024 Jul 5;52(W1):W521-W525. doi:
953 10.1093/nar/gkae241. PMID: 38597606; PMCID: PMC11223882.
954 **Maeda K, Sumita T, Nishi O, Sushida H, Higashi Y, Nakagawa H, Suzuki T, Iwao E,**
955 **Fanani MZ, Nishiya Y, Iida Y.** 2025. Adaptive evolution of sesquiterpene
956 deoxyphomenone in mycoparasitism by *Hansfordia pulvinata* associated with horizontal
957 gene transfer from *Aspergillus* species. *mBio*. 2025 Apr 9;16(4):e0400724. doi:
958 10.1128/mbio.04007-24. Epub 2025 Mar 20. PMID: 40111082; PMCID: PMC11980549.
959 **Mesarich CH, Griffiths SA, van der Burgt A, Okmen B, Beenen HG, Etalo DW, Joosten**
960 **MH, de Wit PJGM.** 2014. Transcriptome sequencing uncovers the *Avr5* avirulence gene
961 of the tomato leaf mold pathogen *Cladosporium fulvum*. *Molecular Plant-Microbe*
962 *Interactions*. 2014 Aug;27(8):846-57. doi: 10.1094/MPMI-02-14-0050-R. PMID:
963 24678832.
964 **Mesarich CH, Ökmen B, Rovenich H, Griffiths SA, Wang C, Karimi Jashni M,**
965 **Mihajlovski A, Collemare J, Hunziker L, Deng CH,** et al. 2018. Specific
966 Hypersensitive Response-Associated Recognition of New Apoplastic Effectors from
967 *Cladosporium fulvum* in Wild Tomato. *Molecular Plant-Microbe Interactions*. 2018
968 Jan;31(1):145-162. doi: 10.1094/MPMI-05-17-0114-FI. Epub 2017 Nov 16. PMID:
969 29144204.

970 **Mesarich CH, Barnes I, Bradley EL, de la Rosa S, de Wit PJGM, Guo Y, Griffiths SA,**
971 **Hamelin RC, Joosten MHAJ, Lu M,** et al. 2023. Beyond the genomes of *Fulvia fulva*
972 (syn. *Cladosporium fulvum*) and *Dothistroma septosporum*: New insights into how these
973 fungal pathogens interact with their host plants. *Molecular Plant Pathology*. 2023
974 May;24(5):474-494. doi: 10.1111/mpp.13309. Epub 2023 Feb 15. PMID: 36790136;
975 PMCID: PMC10098069.
976 **Mesny F, Wolf V, López-Moral A, Kraege A, Punt W, Park J, Zhu J, Sato Y, Thomma**
977 **BPHJ.** 2024. Plant-associated fungi co-opt ancient antimicrobials for host manipulation.
978 *bioRxiv*. Preprint posted online 2024 Jan 4. doi:10.1101/2024.01.04.574150.
979 **Mirdita M, Schütze K, Moriwaki Y, Heo L, Ovchinnikov S, Steinegger M**. 2022.
980 ColabFold: making protein folding accessible to all. *Nature Methods*. 2022
981 Jun;19(6):679-682. doi: 10.1038/s41592-022-01488-1. Epub 2022 May 30. PMID:
982 35637307; PMCID: PMC9184281.
983 **Mistry J, Chuguransky S, Williams L, Qureshi M, Salazar GA, Sonnhammer ELL,**
984 **Tosatto SCE, Paladin L, Raj S, Richardson LJ**, et al. 2021. Pfam: The protein families
985 database in 2021. *Nucleic Acids Research*. 2021 Jan 8;49(D1):D412-D419. doi:
986 10.1093/nar/gkaa913. PMID: 33125078; PMCID: PMC7779014.
987 **Moormann J, Heinemann B, Hildebrandt TM.** 2022. News about amino acid metabolism
988 in plant-microbe interactions. *Trends in Biochemical Sciences*. 2022 Oct;47(10):839-850.
989 doi: 10.1016/j.tibs.2022.07.001. Epub 2022 Aug 1. PMID: 35927139.
990 **Oome S, Raaymakers TM, Cabral A, Samwel S, Böhm H, Albert I, Nürnberger T, Van**
991 **den Ackerveken G.** 2014. Nep1-like proteins from three kingdoms of life act as a
992 microbe-associated molecular pattern in *Arabidopsis*. *Proceedings of the National*
993 *Academy of Sciences, USA*. 2014 Nov 25;111(47):16955-60. doi:
994 10.1073/pnas.1410031111. Epub 2014 Nov 3. PMID: 25368167; PMCID: PMC4250136.
995 **Peresse M, Le Picard D.** 1980. *Hansfordia pulvinata*, mycoparasite destructeur du
996 *Cladosporium fulvum*. *Mycopathologia* 1980. 71:23–30.
997 **Qutob D, Kamoun S, Gijzen M.** 2002. Expression of a *Phytophthora sojae* necrosis-
998 inducing protein occurs during transition from biotrophy to necrotrophy. *The Plant*
999 *Journal*. 2002 Nov;32(3):361-73. doi: 10.1046/j.1365-313x.2002.01439.x. PMID:
1000 12410814.
1001 **Qutob D, Kemmerling B, Brunner F, Küfner I, Engelhardt S, Gust AA, Luberacki B,**
1002 **Seitz HU, Stahl D, Rauhut T,** et al. 2006. Phytotoxicity and innate immune responses

1003 induced by Nep1-like proteins. *The Plant Cell*. 2006 Dec;18(12):3721-44. doi:
1004 10.1105/tpc.106.044180. Epub 2006 Dec 28. PMID: 17194768; PMCID: PMC1785393.
1005 **R Core Team R.** 2024. *R: a language and environment for statistical computing*. Vienna,
1006 Austria: R Foundation for Statistical Computing.
1007 **Rocafort M, Fudal I, Mesarich CH.** 2020. Apoplastic effector proteins of plant-associated
1008 fungi and oomycetes. *Current Opinion in Plant Biology*. 2020 Aug;56:9-19. doi:
1009 10.1016/j.pbi.2020.02.004. Epub 2020 Apr 2. PMID: 32247857.
1010 **Rooney HC, Van't Klooster JW, van der Hoorn RA, Joosten MH, Jones JD, de Wit**
1011 **PJGM.** 2005. Cladosporium Avr2 inhibits tomato Rcr3 protease required for *Cf-2*-
1012 dependent disease resistance. *Science*. 2005 Jun 17;308(5729):1783-6. doi:
1013 10.1126/science.1111404. Epub 2005 Apr 21. Erratum in: Science. 2005 Oct
1014 7;310(5745):54. PMID: 15845874.
1015 **de la Rosa S, Schol CR, Ramos Peregrina Á, Winter DJ, Hilgers AM, Maeda K, Iida Y,**
1016 **Tarallo M, Jia R, Beenen HG,** et al. 2024. Sequential breakdown of the *Cf-9* leaf mold
1017 resistance locus in tomato by *Fulvia fulva*. *New Phytologist*. 2024 Aug;243(4):1522-
1018 1538. doi: 10.1111/nph.19925. Epub 2024 Jun 24. PMID: 38922927.
1019 **Seidl MF, Van den Ackerveken G.** 2019. Activity and Phylogenetics of the Broadly
1020 Occurring Family of Microbial Nep1-Like Proteins. *Annual Review of Phytopathology*.
1021 2019 Aug 25;57:367-386. doi: 10.1146/annurev-phyto-082718-100054. Epub 2019 Jul 5.
1022 PMID: 31283435.
1023 **Shabab M, Shindo T, Gu C, Kaschani F, Pansuriya T, Chintha R, Harzen A, Colby T,**
1024 **Kamoun S, van der Hoorn RA.** 2008. Fungal effector protein AVR2 targets
1025 diversifying defense-related cys proteases of tomato. *The Plant Cell*. 2008
1026 Apr;20(4):1169-83. doi: 10.1105/tpc.107.056325. Epub 2008 Apr 30. PMID: 18451324;
1027 PMCID: PMC2390736.
1028 **Shimodaira H.** 2002. An approximately unbiased test of phylogenetic tree selection. Syst
1029 Biol. Jun;51(3):492-508. doi: 10.1080/10635150290069913. PMID: 12079646.
1030 **Snelders NC, Rovenich H, Petti GC, Rocafort M, van den Berg GCM, Vorholt JA,**
1031 **Mesters JR, Seidl MF, Nijland R, Thomma BPHJ.** 2020. Microbiome manipulation
1032 by a soil-borne fungal plant pathogen using effector proteins. *Nature Plants*. 2020
1033 Nov;6(11):1365-1374. doi: 10.1038/s41477-020-00799-5. Epub 2020 Nov 2. PMID:
1034 33139860.
1035 **Snelders NC, Rovenich H, Thomma BPHJ.** 2022. Microbiota manipulation through the
1036 secretion of effector proteins is fundamental to the wealth of lifestyles in the fungal

1037 kingdom. *FEMS Microbiology Reviews*. 2022 Sep 2;46(5):fuac022. doi:
1038 10.1093/femsre/fuac022. PMID: 35604874; PMCID: PMC9438471.
1039 **Stamatakis A.** 2014. RAxML version 8: a tool for phylogenetic analysis and post-analysis of
1040 large phylogenies. *Bioinformatics*. May 1;30(9):1312-3. doi:
1041 10.1093/bioinformatics/btu033. Epub 2014 Jan 21. PMID: 24451623; PMCID:
1042 PMC3998144.
1043 **Solomon PS, Oliver RP.** 2001. The nitrogen content of the tomato leaf apoplast increases
1044 during infection by *Cladosporium fulvum*. *Planta*. 2001 Jun;213(2):241-9. doi:
1045 10.1007/s004250000500. PMID: 11469589.
1046 **Sonawala U, Dinkeloo K, Danna CH, McDowell JM, Pilot G.** 2018. Review: Functional
1047 linkages between amino acid transporters and plant responses to pathogens. *Plant*
1048 *Science*. 2018 Dec;277:79-88. doi: 10.1016/j.plantsci.2018.09.009. Epub 2018 Sep 19.
1049 PMID: 30466603.
1050 **Sperschneider J, Dodds PN.** 2022. EffectorP 3.0: Prediction of Apoplastic and Cytoplasmic
1051 Effectors in Fungi and Oomycetes. *Molecular Plant-Microbe Interactions*. 2022
1052 Feb;35(2):146-156. doi: 10.1094/MPMI-08-21-0201-R. Epub 2022 Feb 1. PMID:
1053 34698534.
1054 **Sperschneider J, Catanzariti AM, DeBoer K, Petre B, Gardiner DM, Singh KB, Dodds**
1055 **PN, Taylor JM**. 2017. LOCALIZER: subcellular localization prediction of both plant
1056 and effector proteins in the plant cell. *Scientific Reports*. 2017 Mar 16;7:44598. doi:
1057 10.1038/srep44598. PMID: 28300209; PMCID: PMC5353544.
1058 **Stergiopoulos I, Kourmpetis YA, Slot JC, Bakker FT, De Wit PJ, Rokas A**. 2012. In
1059 silico characterization and molecular evolutionary analysis of a novel superfamily of
1060 fungal effector proteins. *Molecular Biology and Evolution*. 2012 Nov;29(11):3371-84.
1061 doi: 10.1093/molbev/mss143. Epub 2012 May 23. PMID: 22628532.
1062 **Sushida H, Sumita T, Higashi Y, Iida Y.** 2019. Draft Genome Sequence of *Dicyma*
1063 *pulvinata* Strain 414-3, a Mycoparasite of *Cladosporium fulvum*, Causal Agent of
1064 Tomato Leaf Mold. *Microbiology Resource Announcements*. 2019 Aug 29;8(35):e00655-
1065 19. doi: 10.1128/MRA.00655-19. PMID: 31467096; PMCID: PMC6715866.
1066 **Tanaka S, Wada K, Katayama M, Marumo S**. 1984. Isolation of Sporogen-AO1, a
1067 sporogenic substance, from *Aspergillus oryzae*. A*gricultural and biological chemistry*.
1068 1984;48(12):3189–3191. doi:10.1271/bbb1961.48.3189.

1069 **Tanaka S, Wada K, Marumo S, Hattori H.** 1984. Structure of sporogen-ao 1, a sporogenic
1070 substance of *Aspergillus oryzae*. *Tetrahedron Letters*. 1984;25(51):5907–5910.
1071 doi:10.1016/S0040-4039(01)81717-2.
1072 **Tang D, Chen M, Huang X, Zhang G, Zeng L, Zhang G, Wu S, Wang Y.** 2023. SRplot:
1073 A free online platform for data visualization and graphing. *PLoS One*. 2023 Nov
1074 9;18(11):e0294236. doi: 10.1371/journal.pone.0294236. PMID: 37943830; PMCID:
1075 PMC10635526.
1076 **Teufel F, Almagro Armenteros JJ, Johansen AR, Gíslason MH, Pihl SI, Tsirigos KD,**
1077 **Winther O, Brunak S, von Heijne G, Nielsen H.** 2022. SignalP 6.0 predicts all five
1078 types of signal peptides using protein language models. *Nature Biotechnology*. 2022
1079 Jul;40(7):1023-1025. doi: 10.1038/s41587-021-01156-3. Epub 2022 Jan 3. PMID:
1080 34980915; PMCID: PMC9287161.
1081 **Thomma BP, VAN Esse HP, Crous PW, DE Wit PJ.** 2005. *Cladosporium fulvum* (syn.
1082 *Passalora fulva*), a highly specialized plant pathogen as a model for functional studies on
1083 plant pathogenic Mycosphaerellaceae. *Molecular Plant Pathology*. 2005 Jul 1;6(4):379-
1084 93. doi: 10.1111/j.1364-3703.2005.00292.x. PMID: 20565665.
1085 **Tirilly Y, Kloosterman J, Sipma G, Kettenes-Van Den Bosch JJ.** 1983. A fungitoxic
1086 sesquiterpene from *Hansfordia pulvinata*. *Phytochemistry*. 1983;22(9):2082–2083.
1087 doi:10.1016/0031-9422(83)80051-X.
1088 **Tünnermann L, Colou J, Näsholm T, Gratz R.** 2022. To have or not to have: expression of
1089 amino acid transporters during pathogen infection. *Plant Molecular Biology*. 2022
1090 Jul;109(4-5):413-425. doi: 10.1007/s11103-022-01244-1. Epub 2022 Feb 1. PMID:
1091 35103913; PMCID: PMC9213295.
1092 **Watanabe H, Horinouchi H, Muramoto Y, Ishii H.** 2017. Occurrence of azoxystrobin-
1093 resistant isolates in *Passalora fulva*, the pathogen of tomato leaf mold disease. *Plant*
1094 *Pathology*. 2017;66(9):1472–1479. doi:10.1111/ppa.12701.
1095 **de Wit PJGM, van der Burgt A, Ökmen B, Stergiopoulos I, Abd-Elsalam KA, Aerts AL,**
1096 **Bahkali AH, Beenen HG, Chettri P, Cox MP**, et al. 2012. The genomes of the fungal
1097 plant pathogens *Cladosporium fulvum* and *Dothistroma septosporum* reveal adaptation to
1098 different hosts and lifestyles but also signatures of common ancestry. *PLOS Genetics*.
1099 2012;8(11):e1003088. doi: 10.1371/journal.pgen.1003088. Epub 2012 Nov 29. Erratum
1100 in: PLoS Genet. 2015 Dec 22;11(12):e1005775. doi: 10.1371/journal.pgen.1005775.
1101 PMID: 23209441; PMCID: PMC3510045.

1102 **de Wit PJGM, Joosten MHAJ, Thomma BHPJ, Stergiopoulos I.** 2009. Gene for gene
1103 models and beyond: the *Cladosporium fulvum*–tomato pathosystem. *Plant relationships*.
1104 Berlin, Heidelberg: Springer; 2009. p. 135–156. (The Mycota; vol 5). doi:10.1007/978-3-
1105 540-87407-2_7.
1106 **Wulff BB, Chakrabarti A, Jones DA.** 2009. Recognitional specificity and evolution in the
1107 tomato-*Cladosporium fulvum* pathosystem. *Molecular Plant-Microbe Interactions*. 2009
1108 Oct;22(10):1191-202. doi: 10.1094/MPMI-22-10-1191. PMID: 19737093.
1109 **Yan L, Chen J, Zhang C, Ma Z.** 2008. Molecular characterization of benzimidazole-
1110 resistant isolates of *Cladosporium fulvum*. *Fems Microbiology Letters*. 2008
1111 Jan;278(2):242-8. doi: 10.1111/j.1574-6968.2007.00999.x. PMID: 18096020.
1112 **Yang K, Chen C, Wang Y, Li J, Dong X, Cheng Y, Zhang H, Zhai Y, Ai G, Song Q**, et
1113 al. 2022. Nep1-Like Proteins From the Biocontrol Agent *Pythium oligandrum* Enhance
1114 Plant Disease Resistance Independent of Cell Death and Reactive Oxygen Species.
1115 *Frontiers in Plant Science*. 2022 Mar 4;13:830636. doi: 10.3389/fpls.2022.830636.
1116 PMID: 35310640; PMCID: PMC8931738.
1117 **Zaccaron AZ, Stergiopoulos I.** 2024. Analysis of five near-complete genome assemblies of
1118 the tomato pathogen *Cladosporium fulvum* uncovers additional accessory chromosomes
1119 and structural variations induced by transposable elements effecting the loss of
1120 avirulence genes. *BMC Biology*. 2024 Jan 29;22(1):25. doi: 10.1186/s12915-024-01818-
1121 z. PMID: 38281938; PMCID: PMC10823647.
1122 **Zaccaron AZ, Chen LH, Samaras A, Stergiopoulos I.** 2022. A chromosome-scale genome
1123 assembly of the tomato pathogen *Cladosporium fulvum* reveals a compartmentalized
1124 genome architecture and the presence of a dispensable chromosome. *Microbial*
1125 *Genomics*. 2022 Apr;8(4):000819. doi: 10.1099/mgen.0.000819. PMID: 35471194;
1126 PMCID: PMC9453070.
1127 **Zhang H, Yohe T, Huang L, Entwistle S, Wu P, Yang Z, Busk PK, Xu Y, Yin Y.** 2018.
1128 dbCAN2: a meta server for automated carbohydrate-active enzyme annotation. *Nucleic*
1129 *Acids Research*. 2018 Jul 2;46(W1):W95-W101. doi: 10.1093/nar/gky418. PMID:
1130 29771380; PMCID: PMC6031026.
1131 **Zhang Y, Skolnick J.** 2005. TM-align: a protein structure alignment algorithm based on the
1132 TM-score. *Nucleic Acids Research*. 2005 Apr 22;33(7):2302-9. doi: 10.1093/nar/gki524.
1133 PMID: 15849316; PMCID: PMC1084323.
1134 **Zhou BJ, Jia PS, Gao F, Guo HS.** 2012. Molecular characterization and functional analysis
1135 of a necrosis- and ethylene-inducing, protein-encoding gene family from *Verticillium*

1136 *dahliae*. *Molecular Plant-Microbe Interactions*. 2012 Jul;25(7):964-75. doi:
1137 10.1094/MPMI-12-11-0319. PMID: 22414440.
1138
1139 **FIGURE LEGENDS**
1140 **Fig. 1. *Cladosporium fulvum* parasitized by mycoparasitic fungus *Hansfordia pulvinata*.**
1141 (a) Representative images of a healthy tomato leaf, lesions caused by *C. fulvum* (*on planta*
1142 *Cf*), and lesions covered by white mycelium of *H. pulvinata* (*on planta Cf/Hp*). Tomato
1143 plants were inoculated with *C. fulvum*, and lesions developed after 2 weeks. *H. pulvinata*
1144 was then inoculated onto the diseased leaves, and white mycelia appeared on the lesions a
1145 week after the second inoculation. *In vitro* cultures of *H. pulvinata* (*in vitro Hp*) and *C.*
1146 *fulvum* (*in vitro Cf*) on nylon membranes on water agar after transfer from PDA. *H. pulvinata*
1147 parasitized *C. fulvum* colonies on water agar (*in vitro Cf/Hp*). (b) Scanning electron
1148 micrographs of hyphae of *C. fulvum* and *H. pulvinata* in *in vitro Cf* and *Cf/Hp* conditions. *H.*
1149 *pulvinata* hyphae have penetrated *C. fulvum* hyphae in the *in vitro Cf/Hp* condition. Bar
1150 indicates 10 μm.
1151
1152 **Fig. 2. Differentially expressed genes (DEGs) and enriched KEGG pathways in**
1153 **mycoparasite *Hansfordia pulvinata*.** (a) UpSet plot of DEGs in the *in vitro* and *on planta*
1154 mycoparasitic conditions (*in vitro Cf/Hp* and *on planta Cf/Hp*; Fig. 1a). Connected dots
1155 indicate shared DEGs; Black single dots represent condition-specific DEGs. Vertical bars
1156 show the number of up- and downregulated genes; colored horizontal bars indicate the total
1157 number of DEGs detected in each interaction. (b) Bubble plot of KEGG pathway enrichment
1158 analysis based on the 891 and 557 shared DEGs shown in (a). Keys: color of symbols
1159 indicates significance level of enrichment (–log adjusted *P*); size of symbol indicates the
1160 number of enriched DEGs in each pathway; the symbol indicates the functional class of the
1161 enriched DEGs.
1162
1163 **Fig. 3. A Nep1-like protein (NLP) secreted from the mycoparasite *Hansfordia pulvinata***
1164 **induces a plant-mediated toxicity against spores of *Cladosporium fulvum*.** (a) Workflow
1165 for identifying small secreted proteins synthesized in *H. pulvinata* during mycoparasitism. (b)
1166 MA plot for expression levels of 165 selected genes. Cutoff thresholds are $\log_2$ Fold-change
1167 (±1.0) for *in vitro Cf/Hp* interaction and log Mean (0.3). (c) Phylogenetic tree constructed
1168 based on NLP amino acid sequences using the maximum likelihood method with 1,000
1169 bootstrap replicates. Type I and Type II have two and four cysteine residues, respectively.

1170 Proteins analyzed in this study are in bold. (d) Multiple sequence alignment of NLP using
1171 MAFFT. Conserved residues are highlighted in orange. (e) Transient expression assays of
1172 NLPs in *Nicotiana benthamiana* via agroinfiltration. Chlorosis and necrosis were assessed 14
1173 days after infiltration by trypan blue staining. Similar results were obtained in three
1174 independent experiments; representative results are in Supplementary Fig. S5c. (f) Percentage
1175 germination of conidia of *C. fulvum* after 24-h treatment with apoplastic fluid from *N.*
1176 *benthamiana* leaves that had been infiltrated with different NLPs or buffer. Asterisks indicate
1177 significant differences between treatments determined using Dunnett's or the Mann–Whitney
1178 *U* test.
1179
1180 **Fig. 4. Differentially expressed genes (DEGs) and enriched KEGG pathways in the**
1181 **pathogen *Cladosporium fulvum*.** (a) UpSet plot showing DEGs identified in the *on planta*
1182 *Cf, in vitro Cf/Hp,* and *on planta Cf/HP* conditions (see Fig. 1A). Connected dots indicate
1183 shared DEGs; Black single dots represent condition-specific DEGs. Vertical bars show the
1184 numbers of up- and downregulated genes; colored horizontal bars indicate the total number of
1185 DEGs detected in each condition. (b) Bubble plot of KEGG pathway enrichment analysis
1186 based on the 363 and 158 shared DEGs shown in (a). Keys: color of symbols indicates
1187 significant level of enrichment (–log adjusted *P*); size of symbol indicates the number of
1188 enriched DEGs in each pathway; the symbol indicates the functional class of the enriched
1189 DEGs.
1190
1191 **Fig. 5. Effector genes in the pathogen *Cladosporium fulvum* were highly expressed**
1192 **during mycoparasitism by *Hansfordia pulvinata.*** (a) Functional classification of DEGs
1193 identified for the *on planta Cf*, *in vitro Cf/Hp* and *on planta Cf/Hp* interactions. Red:
1194 upregulated, stable: grey, blue: downregulated. The number of genes assigned to each
1195 category is in parentheses. (b) Heatmap showing expression profiles of effector genes. The
1196 red-to-blue gradient represents up- and downregulated expression, respectively. Genes with
1197 an adjusted *P*-value ≥0.05 are indicated in gray as not detected (ND). Red arrowhead
1198 indicates *Ecp2*. (c) Antimicrobial activity prediction for 56 effector genes upregulated during
1199 the *in vitro Cf/Hp* interaction (determined using the AMAPEC program). Symbols denote
1200 protein location predicted by EffectorP-fungi 3.0.
1201
1202 **Fig. 6. Sequence dissimilarity and structural similarity between *Cladosporium fulvum***
1203 **effector Ecp2 and killer toxin KP4 proteins.** (a) Predicted 3D structure of Ecp2 generated

1204 using AlphaFold2. The color spectrum from blue to red indicates the N- to C-terminal
1205 positions of residues. (b) Structural comparison of Ecp2 with ZtKP4 and UmVKP4 proteins.
1206 The superposition of the aligned proteins was evaluated using TM-align, and the TM-score
1207 and RMSD values are shown. (c) Heatmap showing sequence similarity among Ecp2, ZtKP4,
1208 and UmVKP4 proteins as identified by BLASTp analysis. (d) Conserved motifs of
1209 the proteins identified by MEME motif analysis. (e) Representative tomato leaf from 4-week-
1210 old tomato plant carrying the *Cf-ECP2* resistance gene at 6 days after infiltration with
1211 purified Ecp2 protein produced by *Escherichia coli*. White dotted outline: area infiltrated
1212 with infiltrated with 1 μM Ecp2; black dotted outline: infiltrated with control protein purified
1213 from *E. coli* harboring an empty vector (EV). Numbers in parentheses indicate the number of
1214 leaves with a hypersensitive response (HR) relative to the number of total leaves. (f) *In vitro*
1215 antifungal activity of Ecp2 against *C. fulvum*, *H. pulvinata*, *Alternaria* sp., *Colletotrichum*
1216 *orbiculare*, and *Saccharomyces cerevisiae*. Spores were cultured on 5% potato dextrose agar
1217 with or without Ecp2. Relative hyphal length was determined 4 days after treatment. Bars =
1218 250 μm. Significant differences between EV and Ecp2 treatments were assessed using
1219 Student's t-test, and *p*-values are indicated.
1220
1221 **Fig. 7. Differentially expressed genes (DEGs) and enriched KEGG pathways in tomato**
1222 **plants.** (a) UpSet plot of DEGs in the *on planta Cf* and *on planta Cf/Hp* conditions (see Fig.
1223 1a). Healthy leaves were used as a control. Connected dots indicate shared DEGs; Black
1224 single dots represent condition-specific DEGs. Vertical bars show the number of up- and
1225 downregulated genes; colored horizontal bars indicate the total number of DEGs detected in
1226 each interaction. (b) Bubble plot of KEGG pathway enrichment analysis based on the 1,619
1227 and 2,153 DEGs shown in (a). Keys: color of symbols indicates significance level of
1228 enrichment (–log adjusted *P*); size of symbol indicates the number of enriched DEGs in each
1229 pathway; the symbol indicates the functional class of the enriched DEGs. Stars indicate
1230 pathways highlighted in (c). (c) KEGG pathways involved in amino acid biosynthesis in
1231 tomato.
1232
1233 **Fig. 8. Overview of the tritrophic interaction among tomato plants, pathogen**
1234 ***Cladosporium fulvum*, and mycoparasite *Hansfordia pulvinata*.** *C. fulvum* secretes effector
1235 proteins that function as virulence factors in susceptible tomato cultivars and antifungal
1236 proteins active against other fungi, but act as avirulence factors upon recognition by *Cf*-
1237 resistant cultivars. *H. pulvinata* parasitizes *C. fulvum* and induces the production of apoplastic

1238 antifungal substances in tomato plants via the Nep1-like protein HpNlp1. *H. pulvinata* also
1239 activates the biosynthesis of the antifungal sesquiterpene 13-deoxyphomenone during
1240 mycoparasitism. Other plant defense responses support this biocontrol effect. Pathways
1241 related to amino acid biosynthesis in the three organisms suggest that nutrients from the plant
1242 are supplied to *H. pulvinata*.
1243
1244 **SUPPORTING INFORMATION**
1245 **Fig. S1** Experimental treatments and principal component analysis (PCA) of transcripts from
1246 the mycoparasite *Hansfordia pulvinata* (Hp), the pathogen *Cladosporium fulvum* (Cf), and
1247 tomato plant, *Solanum lycopersicum*.
1248 **Fig. S2** Secondary metabolite biosynthesis gene clusters in the mycoparasite *Hansfordia*
1249 *pulvinata*.
1250 **Fig. S3** Phylogenetic analysis and functional characterization of proteins in fungal species.
1251 **Fig. S4** Structure of HpNlp1.
1252 **Fig. S5** Responses in plant leaves triggered by HpNlp1 protein.
1253 **Fig. S6** Heat map and hierarchical clustering of effector genes expressed in *Cladosporium*
1254 *fulvum*.
1255 **Fig. S7** Structural comparative analysis of Ecp2 with ZtKP4 and UmVKP4.
1256 **Fig. S8** Differentially expressed genes (DEGs) in KEGG pathways detected in tomato plants.
1257 **Table S1** Primer sequences used in this study.
1258 **Table S2** Summary statistics of RNA-seq data and mapping results.
1259 **Table S3** Functional annotation of all genes in *Hansfordia pulvinata* genome.
1260 **Table S4** Predicted gene clusters involved in secondary metabolite biosynthesis in
1261 *Hansfordia pulvinata*.
1262 **Table S5** Small secreted protein-coding genes (≤300 aa) in *Hansfordia pulvinata*.
1263 **Table S6** Key genes encoding secondary metabolism enzymes in *Cladosporium fulvum*.
1264 **Table S7** Effector genes identified in *Cladosporium fulvum*.
1265 **Table S8** Structural homologs of Ecp2 protein identified from PDB25 using the Dali server.
1266 **Table S9** Species possessing homologs of Ecp2 and KP4 proteins.
1267 **Table S10** Log_2 fold-change for defensin-like genes in tomato plants.